ISSN - 2373-7972

AIMS Neuroscience

Volume No. 12
Issue No. 3
September - December 2025

ENRICHED PUBLICATIONS PVT. LTD

S-9, IInd FLOOR, MLU POCKET,
MANISH ABHINAV PLAZA-II, ABOVE FEDERAL BANK,
PLOT NO-5, SECTOR-5, DWARKA, NEW DELHI, INDIA-110075,
PHONE: - + (91)-(11)-47026006

ISSN - 2373-7972

AIMS Neuroscience

Focus and Scope

AIMS Neuroscience is an international Open Access journal devoted to publishing peer-reviewed, high quality, original papers from all areas in the field of neuroscience. The primary focus is to provide a forum in which to expedite the speed with which theoretical neuroscience progresses toward generating testable hypotheses. In the presence of current and developing technology that offers unprecedented access to functions of the nervous system at all levels, the journal is designed to serve the role of providing the widest variety of the best theoretical views leading to suggested studies. Single blind peer review is provided for all articles and commentaries.

Topics are announced at least three months in advance of each issue with the submission date. Up to five articles, limited to 8000 words, will be published with as wide a range of theoretical views as possible on a given topic. Peer review of papers will be done in a month following the specified submission date. For those that are accepted, on-line publication of the uncorrected article occurs within seven days with the final corrected version done in six weeks. During the next month following acceptance, the authors of the articles will write a commentary paper of no more than 2000 words evaluating the other simultaneously published articles vis-á-vis their own, with the goals of synthesis, integration, and expansion where possible. For any obviously incompatible points, authors are asked to provide specific suggestions on ways to empirically address the points to clarify which is likely correct. These commentaries will be published in the next issue. At the time the original articles are published, a general call for additional commentary papers will occur, targeting submission within a month. These will be subjected to peer review and up to five new commentaries will be published the third month. The overall process is designed to foster productive interaction, leading to the generation of hybrid theories and new ideas.

Submission of theoretical papers that do not fall into planned topical areas and represent well-founded novel contributions are also encouraged. An open call for commentaries on the accepted articles will occur with the goal that these be received within a month followed by peer review within 4 weeks. The journal also encourages submission of empirical papers that relate to theory. The previously described rapid review and publication will occur with these articles.

ISSN - 2373-7972

ISSN - 2373-7972

AIMS Neuroscience

(Volume No. 12, Issue No.3, September - December 2025)

Contents

ISSN - 2373-7972

Modulation of brain alpha rhythm and heart rate variability by attention-related mechanisms

Elisa Magosso*, Giulia Ricci and Mauro Ursino
Department of Electrical, Electronic and Information Engineering, Campus of Cesena, University of Bologna, Cesena (FC), Italy

ABSTRACT

According to recent evidence, oscillations in the alpha-band (8–14 Hz) play an active role in attention via allocation of cortical resources: decrease in alpha activity enhances neural processes in task-relevant regions, while increase in alpha activity reduces processing in task-irrelevant regions. Here, we analyzed changes in alpha-band power of 13-channel electroencephalogram (EEG) acquired from 30 subjects while performing four tasks that differently engaged visual, computational and motor attentional components. The complete (visual + computational + motor) task required to read and solve an arithmetical operation and provide a motor response; three simplified tasks involved a subset of these components (visual + computational task, visual task, motor task). Taskrelated changes in alpha power were quantified by aggregating electrodes into two main regions (fronto-central and parieto-occipital), to test regional specificity of alpha modulation depending on the involved attentional aspects. Independent Component Analysis (ICA) was applied to discover the main independent processes accounting for alpha power over the two scalp regions. Furthermore, we performed analysis of Heart Rate Variability (HRV) from one electrocardiogram signal acquired simultaneously with EEG, to test autonomic reaction to attentional loads. Results showed that alpha power modulation over the two scalp regions not only reflected the number of involved attentional components (the larger their number the larger the alpha power suppression) but was also fine-tuned by the nature of the recruited mechanisms (visual, computational, motor) relative to the functional specification of the regions. ICA revealed topologically dissimilar and differently attention-regulated processes of alpha power over the two regions. HRV indexes were less sensitive to different attentional aspects compared to alpha power, with vagal activity index presenting larger changes. This study contributes to improve our understanding of the electroencephalographic and autonomic correlates of attention and may have practical implications in neurofeedback, brain-computer interfaces, neuroergonomics as well as in clinical practice and neuroscience research exploring attention-deficit disorders.

Keywords: electroencephalography; alpha power; attention; Independent Component Analysis; Heart Rate Variability

1. Introduction

Neural oscillations between 8–14 Hz (alpha frequency band) are the prevalent oscillations in the human waking brain and ubiquitous throughout the cortex [1]. In the electroencephalographic recordings (EEG) at the scalp, the largest alpha amplitude is observed over parietal and occipital regions, but alpha

rhythm is also evident over frontal and central sensorimotor regions (also called Rolandic alpha or mu rhythm) [1]. For a long period, alpha activity has been interpreted to reflect default states of cortical "idling" [2]. This interpretation was based on the classical observations that large alpha amplitude is characteristic of resting or deactivated cortical areas (in which no information is currently processed), while alpha is blocked by cortical activation due to sensory and/or motor processing. Contrary to this earlier interpretation of alpha rhythm as a generic "idling" mechanism, evidence has been accumulated in recent years supporting a functional active role of alpha oscillations in information processing and task execution. A strong piece of evidence comes from the observations that alpha activity can exhibit either a decrease (alpha desynchronization) or an increase (alpha synchronization) in amplitude/power in response to a stimulus or task demand [1].

In particular, recent theories postulate that alpha-band oscillations act as a top-down inhibitory mechanism, implicated in attention [3,4]. According to this hypothesis, an increase in alpha amplitude/power reduces information processing in the underlying neural networks; on the other hand, a decrease in alpha amplitude/power enhances information processing in the corresponding circuits. This hypothesis is supported by several studies covering a broad range of different tasks. For instance, a large amount of studies have investigated alpha power modulation in spatial cuing tasks and feature-detection tasks (for a review see [5,6]). Alpha power suppression is larger over regions encoding the task-relevant feature, while alpha power increases over regions processing distracting or interfering features that need to be actively ignored. In other studies, alpha power modulation has been analyzed in the context of problem solving and arithmetic computation [7–9]. Results show that alpha power decreases when subjects become engaged in cognitive demanding tasks, alpha band suppression becoming larger as task complexity increases. Studies investigating working memory, long-term memory, and creative thinking [10–12] (for a compendium also see [6]) show that posterior alpha power increases in time periods related to retention and/or manipulation of internally represented information, suggesting inhibition of interfering external inputs.

In sum, modulations of alpha power are evident as power suppression in regions that are required for task execution (regions whose responsiveness must be enhanced), and as power increase in regions where distracting information has to be suppressed (regions whose receptivity must be inhibited). Hence, alpha activity, by selectively modulating the level of excitation/inhibition of cortical regions, has the function of enhancing neural processes within the task goals and blocking processes outside these goals. Such function can be considered as the operative definition of topdown attention. Indeed, top-down attention can be defined as the mechanism that prioritizes accessing to and processing of that subset of information deemed to be of the highest relevance for successful task completion [6]. Here we refers to

attention as this endogenous (top-down) form of attention (i.e. under executive control), which is distinct from exogenous attention captured in an involuntary fashion. Accordingly, oscillatory alpha activity appears to support top-down attentional processes, its selective modulation shaping the functional architecture of the brain depending on the task at hand [3–6].

The aim of the present work is to contribute to this field by investigating the power changes in on-going alpha activity during tasks that differently engage distinct forms of attention. To this aim, we quantified EEG alpha power during a complete mathematical task involving a visual attentional component (reading numbers and symbols of an arithmetical operation on a computer screen), a computational component (mentally solving the arithmetical operation), and a motor component (selection and pushing of a button). Then, in order to evaluate the impact of each attentional component, we asked the subjects to perform also some simplified tasks decomposing the complete task in its subcomponents (a visual + computational task, a motor task, a visual task); alpha power changes in the simplified tasks were compared with those in the complete task (visual + computational + motor). We posit that this study, by analyzing the relative role of each attentional component to a composite task, may provide a novel contribution to further elucidate the relationship between attention and alpha-band activity. Indeed, our design is at variance with most studies on alpha power in cognitive tasks that often compare different levels of complexity of the same task [8,13–15] or different strategies used for solving the task [7,15], while only few treated decomposition of a composite task into its attentional subcomponents [16]. In particular, based on the hypothesis that alpha suppression is a mechanism that selectively gates cortical information processing and transfer, we investigated two main problems within this study. First, we analyzed the relationship between alpha power and the involved attentional components. In particular, we expect that the larger the number of attentional components (requiring larger excitation and coordination across cortical areas) the lower the alpha power. Moreover, we investigated whether the relationship between alpha power and the four different tasks is the same across the scalp or is modulated differently over different regions, depending on the specific nature of the involved attentional components. We expected a regional specificity of task-related alpha power modulation, supporting the hypothesis that the involved attentional components elicit a differential participation and activation of distinct brain areas. These issues were unraveled by aggregating electrode sites into two main regions of interest for alpha power measurement: parieto-occipital region and fronto-central region.

Second, using Independent Component Analysis (ICA), we investigated whether individual brain processes, more specifically linked to visual-computational or to motor aspects of attention, can be extracted from a low-resolution EEG, for supporting the previous results and for future possible use in neuroengineering tools. Indeed, the possibility of extracting relevant features from low-resolution EEG

is becoming increasingly attractive especially to realize easy-to-use, comfortable, and cheaper systems to be used in practical applications such as neurofeedback, brain computer interfaces, neuroergonomics, neuromarketing [17–19].

As a further point of novelty, in this study we acquired both EEG and ECG during each task and we performed analysis of Heart Rate Variability (HRV), besides quantification of alpha power. As well known, HRV refers to the physiological fluctuations in the heart period reflecting control of the cardiac activity via the sympathetic and parasympathetic branches of the Autonomic Nervous System (ANS). The power spectral density of the HRV presents two main frequency bands of functional interest: the Low Frequency band (LF, 0.04 to 0.15 Hz) interpretable as an index of the sympathetic activity and the High Frequency band (HF, 0.15 to 0.4 Hz) mainly reflecting the parasympathetic component. The LF/HF power ratio is considered a marker of the sympathovagal balance. HRV indexes have been shown to be modulated under tasks requiring attention (see for example [9,13,20]). Thus, as a further purpose of this study we also tested whether the indexes of HRV were sensitive to the engagement of different attentional components and we examined potential correlations between HRV changes and alpha power changes.

2. Materials and methods

2.1. Participants

Thirty healthy subjects (10 females) voluntarily participated in the study. They were recruited among students and employees of the University of Bologna (Italy). Their ages ranged from 20 to 42. Each participant had normal or corrected to normal vision and reported no medical or psychiatric illness. The study was approved by the local ethical committee and all participants gave written informed consent before the beginning of the experiment. All data were analyzed and reported anonymously.

2.2. Experimental protocol

The participant comfortably seated facing a computer monitor at about 50 cm far, in a quite laboratory. They underwent four consecutive experimental sessions, each lasting 15 minutes. Each single experimental session consisted of three phases: a 5-min initial relaxation phase (named R1), a 5-min central task phase (named T), a 5-min final relaxation phase (named R2). The four experimental sessions differed only in the type of the task executed during the central phase; the tasks were designed to include a complete task involving a set of attentional components and three other tasks involving a subset of

these components.

The complete task (Figure 1) consisted in solving inequalities presented on the screen and in providing the response using the mouse. In order to solve the inequality, the participants had to compute the result of an arithmetic operation consisting in the addition/subtraction of four one-digit numbers, and then compare the result with the provided target. They indicated their decision by selecting the appropriate item on the screen (one of the black boxes with the symbols <, =, >), by moving the mouse and pressing the left mouse button. Each inequality was displayed on the monitor until the participant provided the response; immediately after, a new inequality was presented. For each inequality, the four one-digit numbers and the three operators (+ or −) in the arithmetic operation were generated randomly, while the comparison target was generated as a random integer in the range r−3 to r+3, where r represented the correct result of the arithmetic operation. This small range disallowed a comparison target very distant from the possible result, thus precluding trivial solutions. Participants were instructed to answer as correctly and quickly as possible; speeding up the response was also encouraged by the appearance of the time left whenever a new inequality was presented. Response times (i.e. the time from the appearance of a new screen to item selection by mouse clicking) were collected for each subject.

This task included three attentional components: visual (to read numbers and symbols on the screen), computational (to solve the arithmetic operation) and motor (to move and click the mouse for selecting the response).

The mental task (Figure 1) consisted in solving the inequalities displayed on the monitor, without providing any explicit response. Therefore, this task did not require any hand and finger movement, i.e., it included the visual and computational attentional components, but excluded the motor one. The inequalities appeared on the monitor without the items for response selection and succeeded one another every 5 seconds. The time left was updated at each new presentation, in this case too. The numbers and operators in the arithmetic operation, and the comparison target were generated randomly as in the complete task. Participants were instructed to solve the inequalities as correctly and quickly as possible, even if their responses were not collected.

The reading task (Figure 1) was structured as the mental task (inequalities appeared without the response items every 5 seconds), but participants were instructed to just mentally read the numbers presented on the screen, without performing the arithmetic operation and solving the inequalities. Hence, both the computational and motor components were removed and only the visual attentional component was retained.

The finger movement task (Figure 1) consisted in displaying only the three response items (while the arithmetic operation and inequality were not displayed) and requiring the participants to randomly select one item with the mouse approximately every 5–10 seconds. Specifically, subjects were shown the approximate rate of item selection via a short demo by the operator (G.R) (i.e. they did not receive any instruction to count during the finger movement). After participant's selection, the screen was refreshed displaying the three items again for a new selection and updating the time left. Response times (i.e. the time from refreshing of the screen to item selection by mouse clicking) were collected for each subject.

This task excluded the visual and computational components associated with reading the inequalities and solving them, and retained only the visually-guided motor component.

During the two 5-minute relaxation phases, preceding (R1) and following (R2) each task, the same grey screen with the word "RELAX" was continuously displayed, and participants were instructed to relax during such phases maintaining the eyes open.

The four 15-minute experimental sessions were performed consecutively, separated one another by a 10-minute break; the order of the tasks was randomized across participants. During each experimental session, participants were asked to reduce body and head movements at minimum (except hand and finger movement for mouse use when required for task execution), and not to speak. During the 10-minute breaks between sessions, participants were allowed to speak and move on the seat and received the instructions for execution of the following task.

At the end of the four experimental sessions, each participant was interrogated about execution of the mental and reading tasks in order to ensure that he/she had understood correctly the different duty assigned in each of these two tasks and had not performed arithmetic computation during the reading task (in such case, the recording would have been rejected). Each participant confirmed to have performed correctly the two tasks (no recording was rejected). Two-third of them reported to have missed to finish solving inequalities during some trials of the mental task.

After collection of all recordings, we computed the response time averaged across all subjects in the complete task (mean = 6.6 s, Standard Deviation, SD = 3 s, median = 5.9 s) and in the finger task (mean = 4.97 s, SD = 2.9 s, median = 4.6 s) (see Section 4.1 for comments on this).

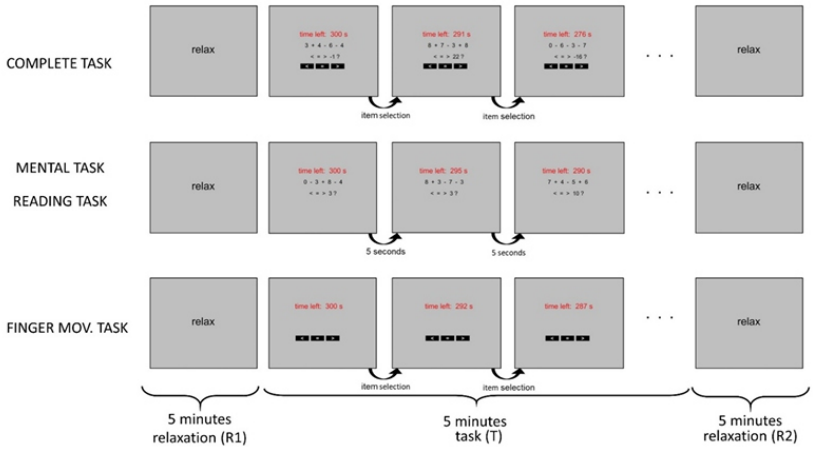

Figure 1. Diagram of the structure of each of the four experimental sessions. Each experimental session included an initial relaxation phase (R1) lasting 5 minutes, a central task (T) lasting 5 minutes, and a final relaxation phase (R2) lasting 5 minutes. Each experimental session differed only for the central task. In the complete task, inequalities appeared on the monitor and the participant had to solve the inequalities (first computing the result of the operation) and select the correct item (one of the black boxes with symbols < = >) with the mouse; after selection, a new inequality appeared. In the mental task, the participant had to solve the inequalities mentally without providing any explicit response. In the reading task, the participant had only to mentally read the numbers appearing on the monitor, without performing any computation. In both the reading and mental tasks, new appearances succeeded every 5 seconds. In the finger movement task, the participant had to randomly choose one selection item, using the mouse (about every 5–10 seconds) and no arithmetic operation was displayed. In each task, the time left within the task phase appeared on the screen. During the relaxation phases, a grey screen with the word 'RELAX' was displayed continuously while participant had to relax.

2.3. EEG and ECG recordings

EEG and ECG were measured simultaneously during the experimental sessions through a Neurowave System (Khymeia, Italy). The EEG signals were recorded using an elastic cap with 13 Ag/AgCl scalp electrodes. For the specific hypotheses of the present study, we focused on anterocentral electrodes (F3, F4, T7, C3, Cz, C4, T8) and on posterior electrodes (PO7, PO3, PO8, Po4, O1, O2). Indeed, these electrodes cover regions linked to different information processing: motor coordination and execution for the more fronto-central regions [21] and visuo-spatial processing for the parieto-occipital regions [22,23]. Therefore, this electrode placement was apt to investigate possible differential effects elicited over these regions by the different examined attentional components. Electrodes were referenced to the right earlobe, and the ground electrode was located on the forehead. One ECG lead was recorded by two

Ag/AgCl electrodes attached just below the right and left collarbones. All electrode impedances was kept below 5 kΩ. During each experimental session, the EEG and ECG data were digitized in continuous recording mode for 15 minutes at a sample frequency of 128 Hz and 16 bit resolution, and with the inclusion of a hardware notch filter eliminating line noise at 50 Hz. Thus, for each participant, four recordings lasting 15 minutes each were produced, relative to the four different tasks (overall 120 recordings were acquired). Furthermore, the 15-min ECG signal of each recording was off-line processed via the Neurowave software for automatic recognition of the R peaks and formation of the time series containing the RR intervals (i.e. intervals between two consecutive peaks), namely the tachogram. Finally, for each participant and each experimental session, the thirteen EEG signals and the tachogram were exported in a Matlab-compatible format for further analysis.

2.4. EEG processing

Processing of the EEG signals of each recording was performed using Matlab (R2016a, The MathWorks Inc., Natick MA). First, the EEG signals were high-pass filtered at 0.75 Hz to eliminate the DC offset and slow drifts. Then, for each participant and each experimental session (complete, mental, reading, finger-movement), the following processing steps were applied to the filtered EEG signals.

2.4.1. Independent Component Analysis (ICA) and artifact removal

The filtered 15-minute EEG signals were decomposed into Independent Components (Ics) using the extended Infomax algorithm [24,25] implemented in the open source EEGLAB Matlab toolbox (https://sccn.ucsd.edu/eeglab/index.php). Independent Component Analysis (ICA) is a widely-used statistical technique to find linear projections of the EEG data that are maximally independent, via minimization of their mutual information. Specifically, ICA finds an unmixing matrix (W) which, when multiplied by the EEG data, provides maximally independent signals (or components, the ICs) whose mixture have been recorded at the scalp. The inverse of the unmixing matrix ($A = W^{-1}$, called mixing matrix) back-projects the ICs into the EEG scalp data. The separated ICs may represent both artefactual signals having non-cortical origin (e.g., potentials produced by eyeball movements, heart contraction, skeletal muscular activity, line noise artifacts etc.), and individual brain-origin signals compatible with synchronized activity within connected patches of the cortex [26]. The ability of ICA to separate non-cortical artefactual components from brain-origin components has made ICA a valuable tool for artifact removal from EEG data [26].

In this study, the unmixing matrix W was attained for the thirteen 15-minute EEG signals (via EEGLAB

toolbox); then, the 15-minute temporal pattern of the thirteen estimated ICs, their Power Spectral Density (PSD), and their scalp maps were computed (outside EEGLAB toolbox). The scalp map of an IC shows the projection weights from the IC to each electrode location, i.e. the weights of the corresponding column of the mixing matrix A. For ICs' PSD computation, we used the same method and parameters adopted for the EEG signals (see below). By visual inspection of ICs' temporal pattern, PSD and scalp maps, we identified and rejected non-cortical ICs related to blinking, lateral eye-movements, heartbeat, muscular activity, and other clear artifacts. This procedure resulted in an average of 3.9 (SD = 0.83) independent components being rejected across all participants and experimental sessions. Artifact-cleaned EEG data were then reconstructed by back-projecting the remaining set of non-artefactual Ics.

Besides using ICA to remove non-brain source processes, here IC decomposition was used also to identify possibly meaningful brain-origin components by evaluating which of these components contributed most strongly to alpha power in the data during the individual tasks (see below for the detailed procedure). In particular, we aimed to assess whether independent components exhibited alpha power modulation more sensitive to the different tasks than undecomposed EEG signals.

2.4.2. Alpha power computation over regions of interest

The artifact-cleaned EEG signals were subdivided into three parts of 5 minutes each, corresponding to the three phases of the session (R1, T, R2). The PSD of each channel over each phase was obtained by applying the Welch's periodogram method, by using a Hamming window of 5 seconds at 50% overlap, zeropadded to 10 s to obtain 0.1 Hz frequency resolution. Then, for our purposes, we topographically aggregated the channels into two regions of interest: a region (FrontoCentral-Temporal, FCT region) including the antero-central channels (F3, F4, T7, C3, Cz, C4, T8) and a region (Parieto-Occipital, PO region) including posterior channels (PO7, PO3, PO8, PO4, O1, O2). The mean PSD over the FCT and PO regions were computed by averaging the PSD across the corresponding channels, separately for each phase R1, T, R2. Then, the power in the alpha band 8-14 Hz was computed over each region of interest and for each phase R1, T, R2. For each region, the alpha power in the R1 phase was used as reference and the alpha power value in each phase was normalized with respect to this reference value. Normalization relative to the initial relaxation phase of each session was done to rule out possible confounding effect of participant's fatigue due to the execution of previous sessions, and to focus only on the changes induced by the specific task.

2.4.3. IC contributions to the alpha power

In order to derive cues on independent processes mainly responsible for the alpha power observed over the two scalp regions, we computed the alpha power ascribed to each (non-artefactual) independent component. To this aim, the single (non-artefactual) IC was back-projected into the scalp channels, and the alpha power over the FCT and PO regions along the entire session duration was computed considering only the single back-projected component. This procedure was repeated for each IC, and the ICs were ranked based on the value of the alpha power they provided, separately for the FCT and PO regions. Next, within each ranking, we considered the two IC components that provided the highest contribution to the alpha power in the FCT ranking (1^IC-FCT, 2^IC-FCT) and in the PO ranking (1^IC-PO, 2^IC-PO). Then, the alpha power of each of these components was computed separately in each phase (R1, T, R2) of the experimental session and normalized with respect to the R1 value used as a reference.

Via this analysis, we aimed to discover individual components mostly accounting for the alpha power observed over the two scalp regions, which may be related to functionally distinct brain processes, and to assess whether these components were more distinctive of specific attentional aspects than undecomposed EEG signals. In perspective, these components may be exploited to drive neuroengineering applications (such as in neuro-ergonomic studies, BCI applications, and so on) without the need to use high-density EEG.

2.5. HRV analysis

For each participant and each experimental session, the following steps were applied to the RR interval time series to derive indexes of HRV.

First, the time series of the RR intervals was processed for recognition and correction of possible artifacts due to participant's movement, equipment failure or others. To this aim, we utilized the open source software ARTiiFACT (http://www.artiifact.de/) [27], that allows detection and treatment of artifacts in the tachogram. Specifically, within ARTiiFACT, the tachogram was submitted to the artifact detection algorithm proposed by Bernston et al. [28]. This is a widely used method for automatic artifact recognition; differently from other methods that detect artifacts as outliers that deviate from the mean/median more than a given threshold, the Berntson's method is based on the distribution of the differences in the RR intervals of the individual subject. Overall, in our RR time series, a limited number of artifacts was detected: 66 out of the 120 examined tachograms had no artifact; 42 tachograms had a percentage of detected artifacts below 1% (mean = 0.3%, SD = 0.25%); 9 tachograms had a parcentage of detected artifacts between 1% and 3% (mean = 1.64%, SD = 0.36%); the remaining 3 tachograms had

a parcentage of detected artifacts ~4.1%, ~4.9%, and ~7%. The detected artifacts in each tachogram were replaced using linear interpolation, within ARTiiFACT software. The artifact-processed tachogram was then elaborated using Matlab. First, it was resampled at 10 Hz using linear interpolation and then low-pass filtered with a cut-off frequency of 0.5 Hz. The interpolated and filtered tachogram was subdivided into three portions each covering 5 minutes, corresponding to the three phases (R1, T, R2) of the experimental session. The PSD of each 5-minute portion was estimated via the periodogram Welch's method using a Hamming window of 100 seconds at 50% overlap, zeropadded to 500 s to obtain 0.002 Hz frequency resolution. The power in the low frequency band (0.04–0.15 Hz, LF power) and in the high frequency band (0.15–0.4 Hz, HF power) was then computed for each phase (R1, T, R2), and the ratio between the LF power and the HF power (LF/HF ratio) was derived too. Likewise the alpha power, the three indexes of HRV (LF power, HF power, LF/HF ratio) were normalized to the corresponding value in the R1 phase considered as the reference value.

2.6. Statistical analyses

Graphpad software (https://www.graphpad.com/) was used for statistical analyses. Statistical analyses were designed in order to:

a) Compare the normalized alpha power changes induced during the complete task with those induced during the other tasks, over each region of interest (FCT and PO) both in the measurement space and in the component (IC) space. Our hypothesis was that regional alpha power might be modulated not only by the number but also by the nature of the involved attentional components, linked to the functional role of the specific region.

b) To compare the normalized changes in the HRV indexes induced during the complete task with those induced during the other tasks. Our hypothesis was that HRV indexes could also depend on the amount of attentional engagement.
c) To explore possible correlation between changes in alpha power and changes in HRV indexes during the tasks.

Hence, the variables under statistical analyses were the normalized alpha powers and the normalized indexes of HRV, during each of the four tasks. Test for Gaussianity of each variable was performed using the omnibus K2 test. The hypothesis of Gaussianity was acceptable for each variable but the normalized LF/HF in the complete and mental tasks ($p < 0.05$). Therefore, the normalized LF/HF index in all sessions was square-root transformed to make it Gaussian in all sessions for parametric comparison.

Repeated measures ANOVA with Greenhouse-Geisser correction for violation of sphericity were used (uncorrected degrees of freedom and corrected probability levels are reported). Onesample t tests and post-hoc paired t tests were Bonferroni corrected for multiple comparisons. Correlation was tested using Pearson's correlation coefficient, with Bonferroni correction for multiple comparisons.

3. Results

3.1. Effect of tasks on alpha power

Figure 2 displays the mean PSD over the FCT and PO regions computed during each phase (R1, T, R2) of the four experimental sessions (complete, mental, reading, finger movement), averaged across participants. First, we can observe that during each initial relaxation phase (R1), the PSD exhibited a peak in the alpha band (8–14 Hz), assuming particularly large values over the PO region (note the different scales used along the y-axis for the two regions). Second, during each task phase (T), the amplitude of the power spectrum in the alpha band showed a dramatic decrease over the PO region and a smaller decrease over the FCT region, compared to the corresponding R1 phase. Finally, during each final relaxation phase (R2), the power spectrum in the alpha band increased again, recovering or slightly overcoming the values in the corresponding R1 phase. These results are in line with the common finding that alpha oscillations are more evident during relaxation and are more prominent in the posterior regions.

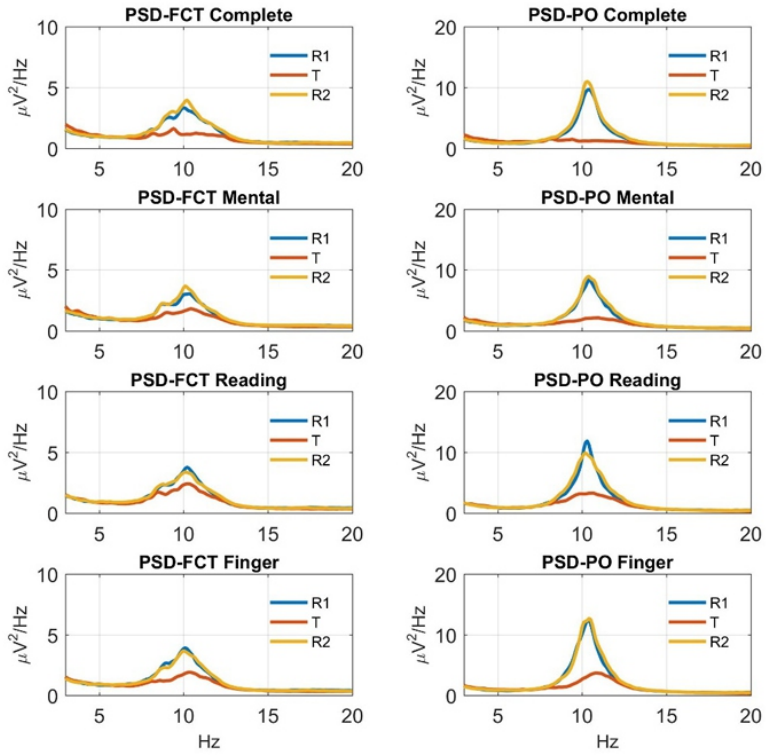

Figure 2. Power spectrum density (PSD) over the FCT region and the PO region computed during each phase (initial relaxation = R1; central task = T; final relaxation = R2) of the four experimental sessions (involving respectively the complete task, the mental task, the reading task, the finger movement task), averaged across the subjects. For each subject, the PSD over the FCT region and PO region were obtained by averaging the PSD of the channels F3, F4, T7, C3, Cz, C4, T8 and of the channels Po3, PO4, PO7, PO8, O1, O2, respectively. A smaller scale along the y-axis was adopted for the PSD over the FCT region in order to allow better appreciation of its modulation across the three phases of each session. The two relaxation phases of each session were characterized by a peak of the power spectrum in the alpha band, with larger values over the PO region. Each task phase was characterized by a decrease of the power spectrum in the alpha band, more consistent over the PO region.

Figure 3 plots the mean (± SE, Standard Error) across all participants of the normalized alpha power in the three phases of each experimental session, separately for the FCT region and the PO region. The alpha power exhibited a fall in all task phases relative to the corresponding R1 phase, assuming values in the range 60% to 80% of the reference value in the FCT region and in the range 45% to 65% in the PO region. Multiple one-sample t tests, applied separately for each region, confirmed that normalized alpha power significantly deviated from the reference value (1) during each task (see Figure 3). During R2, the alpha power recovered the reference value or slightly increased above it (see section Discussion for comments on alpha power rebound in R2).

Interestingly, looking at the values in phase T, it is suggested that the different tasks could modulate differently the alpha power in the two regions: indeed, in the PO region the effect of the complete task appeared closer to that of the mental task, whereas in the FCT region the effect of the complete task was closer to that of the finger movement task.

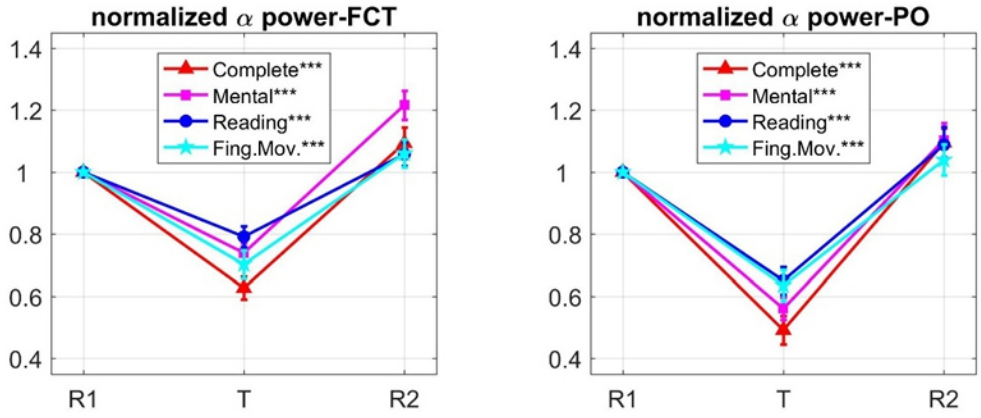

Figure 3. Mean ± standard error (SE, vertical bars) across subjects of the normalized alpha power during each phase (R1, T, R2) of the four experimental sessions, reported separately for the FCT region and the

PO region. Values at R1 coincide with 1 since normalization in each phase of the session was done relative to the alpha power during the corresponding R1 phase (reference phase). In both regions, each task execution (T) induced a significant decrease in alpha power relative to the reference value (multiple one-sample t-tests); asterisks in the legend denote the level of significance (***$p < 0.001$, **$p < 0.01$, *$p < 0.05$; p-values were Bonferroni-corrected for four comparisons). However, the effect of the task type appeared to be non-uniform across the two regions, the different tasks modulating differently the alpha power (the four points in T had a different order in the two plots; see also Table 2).

To investigate the effect of the task's type over each region, a repeated measures one-way ANOVA with task type (complete, mental, reading, finger movement) as within-subject factor was conducted on the normalized alpha powers during the task phases. Results indicated a significant main effect of task type over both the FCT region ($F_{3,87} = 7.810$, $p < 0.001$) and the PO region ($F_{3,87} = 6.734$; $p = 0.002$). Post-hoc paired t-tests were performed comparing the complete task with each of the other tasks, in each region (Table 1). In the FCT region, the complete task came out to be significant different from the reading and mental tasks but not from the finger task, while in the PO region the complete task was significant different from the reading and finger tasks but not from the mental task. Hence, the different tasks impacted unevenly over the two regions, the complete and finger tasks producing similar alpha power modulation over the fronto-central but not the posterior region, whereas the complete and mental task producing similar effects over the posterior but not the fronto-central region. These results suggested that distinct and differently regulated processes contributed to the alpha oscillations over the two regions. To gain cues on this, we performed an analysis at the level of independent components.

Table 1. Results of the post-hoc paired t-tests comparing the complete task against each of the other tasks over each region (FCT and PO) separately (reported p-values are Bonferroni corrected for three comparisons).

	FCT region	PO region
Complete task vs Mental task	$^{**}p = 0.0012$	$p = 0.07$
Complete task vs Reading task	$^{***}p < 0.001$	$^{***}p < 0.001$
Complete task vs Finger task	$p = 0.1$	$^{**}p = 0.006$

The two ICs (1^IC and 2^IC) that mostly explained alpha power over each region were identified per each participant and experimental session (see Material and Methods). Their topographical maps, averaged across participants, are shown in Figure 4. Overall, each of the identified components exhibited averaged scalp distributions quite similar across the four experimental sessions (see the maps

along each column in Figure 4). Importantly, the identified ICs exhibited different scalp distributions depending on the considered region. Notably, among the 480 identified ICs (2 ICs x 2 regions x 4 experimental sessions x 30 participants), the same IC was identified for both the FCT and PO regions (either at the first or second position in the rank) limitedly to 9% of cases. Accordingly, alpha activity over the regions FCT and PO may be mostly ascribed to independent brain processes characterized by different scalp topographies. As to the FCT region, the first contributing IC exhibited a central maximum and symmetrical patterns towards frontal and posterior areas; the second contributing IC had lateral centro-parietal maxima and extended towards posterior-parietal areas. As to the PO region, both the two identified ICs had scalp distribution sharply confined over the posterior areas.

The identified ICs were then analyzed in terms of normalized alpha power changes during each task phase (see Material and Methods). Values (mean ± SE) averaged across participants are plotted in Figure 5. For each IC, multiple one-sample t-tests confirmed significant deviation of normalized alpha power from 1 during each tasks (see results in Figure 5). Plots in Figure 5 suggest that each IC exhibited a pattern of task-dependent alpha modulation similar to that observed at the corresponding channels level (Figure 3). As to the 1^IC-FCT and 2^IC-FCT, the finger task produced an alpha power decrease approaching that induced by the complete task (this is especially evident in the 2^ICFCT). Conversely, as to the 1^IC-PO and 2^IC-PO, the mental task produced the effect closest to the complete task. Repeated measures one-way ANOVA with task type as within-subject factor was applied to normalized alpha power of each IC (in the task phase), showing a main effect of task (1^IC-FCT: $F_{3,87} = 3.124$, $p = 0.037$; 2^IC-FCT: $F_{3,87} = 5.278$, $p = 0.003$; 1^IC-PO: $F_{3,87} = 8.693$, $p < 0.001$; 2^IC-PO: $F_{3,87} = 3.951$, $p = 0.015$). Post-hoc paired t tests (Table 2) proved that the 1^IC-FCT and especially the 2^IC-FCT emphasized the non-significant deviation between the complete and the finger task, maintaining a significant (or close to significance) difference between the complete task and the mental and reading tasks. On the other hand, 1^IC-PO and 2^IC-PO (Table 2) emphasized the non-significant difference between the complete and mental tasks, while presented significant difference of the complete task from the finger and reading tasks.

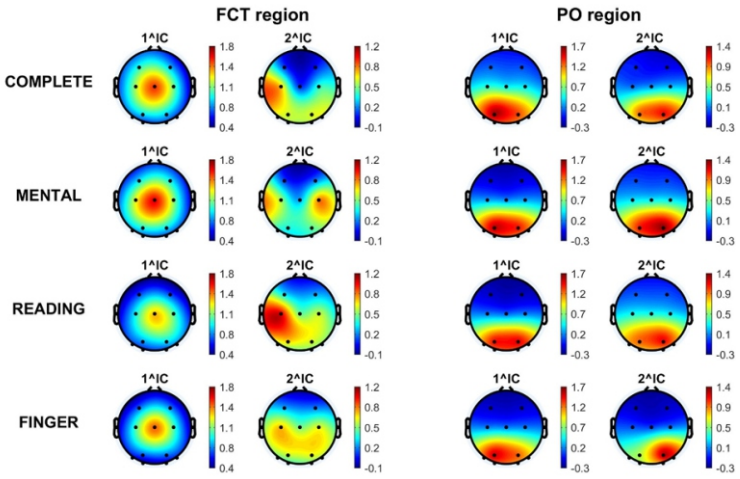

Figure 4. Mean scalp maps averaged across participants showing the projection weights of the two ICs that more strongly contributed to alpha power over the FCT region (the two columns on the left) and over the PO region (the two columns on the right). Each row refers to a specific experimental session. On average, the two ICs explained more than 70% of alpha power over each region respectively, with the first one accounting for about the 50%.

Overall, these results are suggestive of functionally distinct brain processes subtending alpha oscillations over more central regions and more posterior regions; in the former, alpha synchronization appears to be mainly reduced by motor and visuomotor attentional components, whereas in the latter alpha power seems to be mainly reduced by visual-computational attentional components.

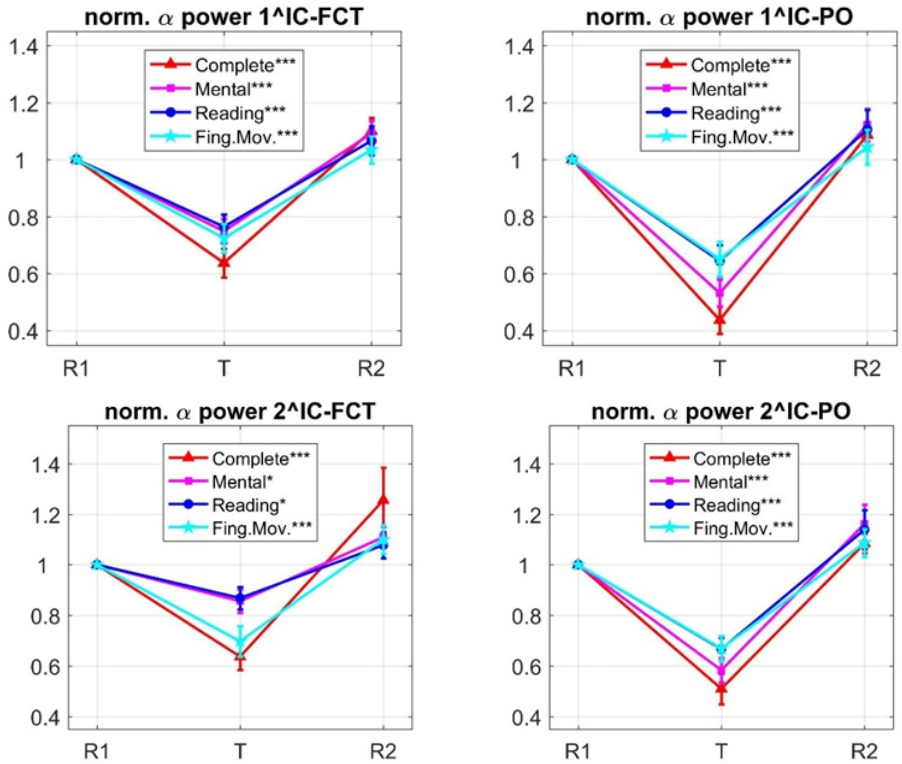

Figure 5. Mean ± standard error (SE, vertical bars) across subjects of the normalized alpha power during each phase (R1, T, R2) of the four experimental sessions, computed on the 1^ and 2^ ICs contributing to FCT alpha power (1^IC-FCT, 2^IC-FCT) and on the 1^ and 2^ ICs contributing to PO alpha power (1^IC-PO, 2^IC-PO). In both regions, each task execution (T) induced a significant decrease in alpha power relative to the reference value (multiple one-sample t-tests); asterisks in the legend denote the level of significance (***p < 0.001, **p <0 .01, *p < 0.05; p-values were Bonferroni-corrected for four comparisons). The components 1^IC-FCT, 2^IC-FCT exhibited task-dependent alpha power modulation (phase T) in line with that observed at the FCT channels, i.e. the complete-task and the finger-task were associated with larger and closer alpha power decrease (especially in the 2^IC-FCT). The components 1^IC-PO and 2^IC-PO (right plots) exhibited task-dependent alpha power modulation consistent to that observed at the PO channels, i.e. the complete task and the mental task were associated with larger and more similar alpha power decrease.

Table 2. Results of the post-hoc paired t-tests performed on the normalized alpha powers of each examined independent component (1^IC-FCT, 2^IC-FCT, 1^IC-PO, 2^IC-PO); the tests compared the effect of the complete task against each of the other tasks, separately for each component (reported p-values are Bonferroni corrected for three comparisons).

	1^IC-FCT	2^IC-FCT	1^IC-PO	2^IC-PO
Complete task vs Mental task	$p = 0.061$	$^{**}p = 0.006$	$p = 0.13$	$p = 0.756$
Complete task vs Reading task	$^{*}p = 0.035$	$^{**}p = 0.005$	$^{***}p < 0.001$	$^{*}p = 0.024$
Complete task vs Finger task	$p = 0.3249$	$p > 0.999$	$^{***}p < 0.001$	$^{*}p = 0.014$

3.2. Effect of tasks on HRV and correlation tests between HRV and alpha power

Figure 6 shows the mean (± SE) across participants of the HRV indexes (LF power, HF power, ratio LF/HF) in the three phases of each experimental session, normalized relative to the corresponding R1 phase. Moreover, the figure reports the results of multiple one-sample t-tests performed for each index during the tasks. During task execution HRV tended to reduce especially in the HF band, while the LF power decreased to a lower extent. This was reflected in a tendency of LF/HF ratio to increase.

Repeated measures one-way ANOVA with task type as within-subject factor were applied to each HRV index during the task phases, revealing no main effect of task on any index (LF power: $F_{3, 87} = 1.589$, $p = 0.206$; HF power: $F_{3, 87} = 0.924$, $p = 0.419$; LF/HF ratio $F_{3, 87} = 0.478$, $p = 0.687$). Hence, although the

mental and complete tasks seemed to produce larger effects compared to the reading and finger tasks both in the LF and HF bands (Figure 6), there were not significant differences across the tasks. We can conclude that HRV indexes are less sensitive to different task types involving different attentional components, compared to EEG alpha power indexes. Finally, we tested the correlation across all subjects between the HRV indexes (LF index, HF index) and each of the alpha power indexes (normalized alpha power of the two scalp regions and normalized alpha power of the four selected independent components), separately during each task; that is, six Pearson's tests were performed for each HRV index during each task, with Bonferroni corrected p-value. No significant correlation was found with alpha power for either LF index (minimum corrected p-value = 0.14) or HF index (minimum corrected p-value = 0.23), in any task.

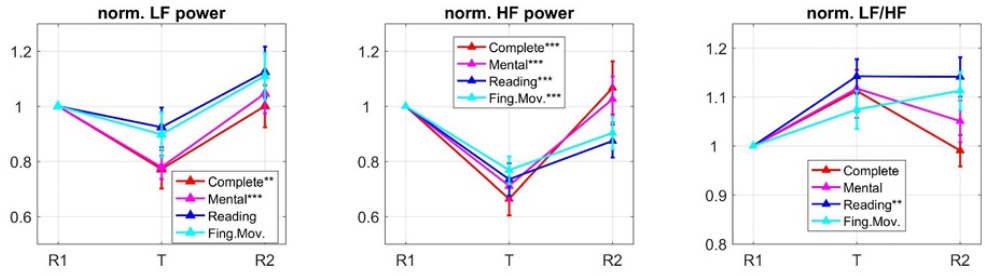

Figure 6. Mean ± standard error (SE, vertical bars) across subjects of the normalized HRV indexes (LF power, HF power and the ratio LF/HF) during each phase (R1, T, R2) of the four experimental sessions. The normalization was done relative to each corresponding R1 phase (producing values equal to 1 in R1). The values plotted in the rightmost plot refer to root-square transformation of the normalized LF/HF index, to make it Gaussian for parametric analyses. Overall, during each task execution HF power decreased more than LF power, and LF/HF ratio tended to increase.

4. Discussion

In this study, we investigated the differential effect of tasks involving different combinations of attentional components (visual, computational, motor) on both brain activity and autonomic nervous activity. The effect on brain activity was analyzed through quantification of task-related EEG alphapower changes in two regions of interest over the scalp (a fronto-central region and a posterior region). Moreover, independent component decomposition of EEG data was applied in order to get cues on possibly distinct brain processes contributing to alpha-power modulation and to extract relevant individual components for future possible uses in neuro-engineering applications. The effects on autonomic nervous activity were analyzed via HRV indexes (the power of the tachogram spectrum in the LF and HF bands) and quantification of their task-related changes. Finally, the correlation between alpha power measurements and HRV indexes during the attentional tasks was tested.

4.1. Task-related modulation of alpha power

The first general result of our study is that a significant alpha power decrease, relative to the baseline (the pre-task relaxation phase), was observed (Figure 3) over both the front-central and the parieto-occipital regions during each task. Alpha power increase was never observed on either scalp regions during the examined tasks, in line with previous studies showing that increase in alpha activity occurs when distracting or confounding information must be actively blocked (e.g., when attended one side of the space while distracting information on the other side must be ignored), a condition not occurring in our tasks. The significant alpha power decrease observed over both scalp regions suggests that the influence of the attentional components involved in each task was widely distributed, each task requiring the co-participation of several areas and brain processes. This broad alpha power suppression observed in all examined tasks is also in line with previous findings. Previous EEG studies involving mental arithmetic (specifically addition and subtraction) found alpha power decrease especially in parietoccipital regions but also in frontocentral regions [7–9,15]. Interestingly, widespread alpha power suppression occurred in relatively complex tasks (e.g., addition of two-digits numbers, operations with more than two operands, operations involving subtraction), similar to the operations used in this study, while it was less evident in simpler task (e.g., 2 + 3). Fernandez et al. [16] during a task involving the reading of multiple digit numbers observed a significant alpha power decrease in all 19 EEG channels (located according to the traditional 10/20 system). In motor tasks, alpha power suppression was not confined over motor areas [29,30], especially when also sensory information (e.g., tactile and/or visual) needs to be integrated, as actually occurred in our finger movement task.

Despite the generalized alpha power decrease over both regions during the tasks, a difference emerged between the two regions. This difference appears consistent with the main functional role of the underlying cortical areas. Precisely, in both regions the complete task (having the larger number of attentional components) tended to produce the largest alpha power suppression and the reading task (involving only visual component) the lowest alpha power suppression, while the other two tasks (the finger movement and mental tasks) were collocated approximately in between. However, while in the fronto-central region, the complete task presented larger (and significant) deviation from both the mental and reading tasks, it presented a smaller deviation (not reaching significance) from the finger task. On the other hand, while in the parieto-occipital region the complete task showed larger and significant deviation from both the finger and reading tasks, it showed a smaller deviation (not reaching significance) from the mental task. Overall, these results are suggestive of a graded relationship between the number of involved attentional components and extent of alpha suppression (the larger the number of attentional components the larger the suppression in alpha power).

However, this graded relationship did not have a uniform pattern across brain regions, but it was fine-tuned based on the main functional role of the underlying cortical areas. These observations are in line with the hypothesis that alpha modulates attentional cortical resource allocation. Indeed, a task entailing a larger numbers of attentional components will engage several cortical areas, requiring disinhibition of more numerous and larger assemblies of neurons (so that they may become entailed in specific information processing) and thus in general will provide larger alpha power suppression. However, the involved attentional components will mainly affect the areas more strongly implicated in the corresponding information processing, and to a less extent more marginal areas. Indeed, recent EEG studies suggest that the posterior parietal and occipital regions are involved in visuo-spatial processing of stimuli [22], spatial representation of numbers [23] and complex (vs simple) arithmetic problems requiring procedural strategies [7,31]. Accordingly, in the present study alpha power over these areas appeared to be strongly affected by the visual and computational attentional components of the complete and mental tasks, while the reading task and the finger movement task required relatively lower recruitment of these areas. Conversely, frontocentral areas are strongly implicated in sensory-motor integration and motor execution, and therefore they were strongly entailed by the visuo-motor component of both the complete task and the finger task (while their recruitment in the reading and mental task was relatively lower).

Motivated by this interpretation, we extracted independent components that mainly contributed to EEG power over each region. Based on the previous results, we expected that the components mainly responsible for alpha power over each region were distinct and differently attentionmodulated, possibly being related to brain processes that subserve distinct functions. Indeed, we found that the two main contributions to alpha power over the fronto-central channels and the parieto-occipital channels were provided by different independent components, having scalp topography and task-related power modulation (Figures 4 and 5) more compatible with sensorymotor and motor processes on one hand, and visuo-spatial-calculation processes on the other hand. Of course, association between scalp topographies and cerebral processes/functions remains at a speculative level here, due to the unfeasibility of applying algorithms that estimate (distributed or concentrated) cortical sources, because of the limited number of electrodes. However, we provide a cautious neurophysiological explanation of these analyzed independent components, which undoubtedly requires further investigation and evidence. As to the 1^IC-FCT, it could be related to a multisensory-motor process (localized in frontal or anterior-parietal cortex), supporting the integration of multisensory (tactile, visual, proprioceptive, etc.) information—but also endogenously generated information (e.g., computation result)—with motor behavior and response. Indeed, as to its task-related alpha power modulation, the largest alpha power suppression was observed in the complete task, where all the previous information must be integrated,

and was found to exhibit the lowest deviation from the finger movement task where still multisensory and motor information needed to be integrated. The 2^IC-FCT might be implicated in final motor execution, located in the motor cortex; indeed its alpha power suppression was the largest in the complete and finger tasks and exhibited very similar value in these two cases. As concerning the two main components of PO alpha power (1^IC-PO and 2^IC-PO), they could be related to occipital and posterior-parietal processes that become triggered in visuo-spatial processing and in mathematical cognition; their alpha power suppression is most prominent (and not different) in the complete and mental tasks. The similarity of the averaged scalp maps of the two independent components 1^IC-PO and 2^IC-PO (Figure 4) deserves a clarification. Actually, for each single subject, these two components turned out to have scalp maps with a pretty clearly lateralized peak, located posteriorly on the left (over positions Po3, PO7, O1) for one component, and on the right (over position PO4, PO8, O2) for the other, each possibly reflecting (visuospatial/computational) processes relative to one hemisphere. However, there was not consistency across subjects and tasks concerning the rank in contributing to PO alpha power (1^ or 2^ position) and the left- or right-peaking of these two components: sometimes, the left- (right-) peaking component occurred to provide the first (second) contribution to PO alpha power and sometimes the vice-versa occurred. Therefore, when averaging their scalp maps across subjects, lateralization tends to disappear creating a pretty uniform (with just a small left or right bias) posterior distribution.

Two further points regarding alpha power changes obtained in our study deserve comments.

First, in the mental and reading tasks, there was a predefined time window (5 s) imposing the rate of screen refresh (0.2 Hz), i.e. the rate of trials, while in the complete and finger tasks a predefined time window was not imposed possibly slowing the average rate of trials (defined by the average response time, see Section 2.2.). This task difference might constitute a source of bias of alpha power, by reducing the level of stress and thus producing underestimation of alpha power decrease in the complete and finger tasks compared to the mental and reading tasks. While we cannot exclude this possibility, we are inclined to consider this effect insignificant. Indeed, the finger task turned out to be characterized by an average rate of trials close to 0.2 Hz (as the mental and reading tasks). Moreover, we have verified that in the finger task, there was not correlation between the rate of item selection (i.e. the rate of finger movement) and the alpha power decrease across the thirty participants ($p > 0.39$). For what concerns the complete task, the average rate of trials was effectively lower (average response time = 6.6 s); this might have introduced a positive bias (reduced alpha decrease) compared to the mental task in particular, as both tasks required to solve inequalities. However, in the mental task, each assigned time window was only devoted to solve the inequality (without spending time for identifying the item matching the solution, moving the mouse over it, clicking the mouse); moreover, most of participants admitted to have

not finished solving inequalities in some trials of the mental task. Accordingly, we reasonably claim that the mental task did not involve additional workload and attentional effort in inequality solving compared to the complete task.

A second point concerns the restriction of our analysis to alpha power changes during the tasks, whereas also analysis of alpha rebound in R2 (relax post-task) might potentially provide further information about the involved attentional processes. Actually, statistical analyses applied to normalized alpha powers in the R2 phase failed to identify significant deviation from R1 phase (indeed, significance occurred only for R2 alpha rebound in the FCT region as to the mental task) and failed to identify differences across tasks. Further studies are necessary to assess whether the absence of task effect in R2 at scalp level is a genuine result, or rather a task effect in R2 occurs at cortical level and is masked by the volume conduction phenomenon and low electrode spatial resolution (maybe the task effect at phase R2 being of lower magnitude compared to the task effect at phase T).

Overall, we posit that the present study not only provide an incremental contribution to our knowledge of the electroencephalographic features of attention, and of their modulation by the number and nature of involved attentional components, but may have practical implications, too. Indeed, the obtained results suggest that even the use of a limited number of electrodes, as adopted in clinical settings or in neuro-engineering applications, if combined with independent component analysis, may allow the extraction of independent signals that better characterize either visualcomputational aspects of attention or motor aspects of attention. This can open interesting possibilities in future applications where extracting relevant attentional features (more motor-related or cognitive-related) from a simple-to-use EEG system may have significant practical value, such as in neuroergonomics applications (e.g., in work and driving settings), in BCI applications, but also in clinical applications e.g. for monitoring attentional level in subjects with attention-deficit disorders.

4.2. Task-related modulation of HRV indexes

Our results concerning HRV indexes indicated a general decrease in HRV during task execution, characterized by a more relevant decrease in the HF band than the LF band and a consequent unbalancing towards sympathetic activity relative to parasympathetic activity (as indicated by the tendency of LF/HF ratio to increase). Reduction in HRV (especially in vagally-mediated HRV) during attentional demanding tasks has been documented in literature [9,13,20,32,33]. Furthermore, some of these studies also showed sensitivity of HRV indexes to different levels of attention or workload. In our study, although tasks could induce significant changes in the HRV indexes compared to baseline, none of

the examined indexes exhibited significant differences across the tasks (see section Results). However, in the previous studies, participants performed each task for more than 10 minutes, while here each task lasted 5 minutes. A possibility is that changes in autonomic regulation of HRV might require more time to develop completely.

When correlation was tested between alpha power indexes and HRV indexes, no significant results was obtained. Investigating the relationship between oscillatory neural activity and HRV in relaxation and attention condition may contribute to disclose cortical processes influencing cardiovascular control in attentional states, and to improve our understanding on how our brain operates to react to attentional loads not only at central but also at peripheral level. Within this issue, some previous studies found significant correlation between EEG oscillatory activity and indexes of cardiac autonomic activity both in attentional states [9,34] and during relaxation [35,36]. However, in most cases, only low magnitude of correlation (~0.3, 0.4) was found. We claim that understanding the information dynamics between brain and heart will benefit from the use of more sophisticated methods of analysis, able to capture not only linear, but also non-linear associations, such as the recent emerging methods based on transfer entropy to investigate the causal relationship among temporal series [37].

Finally, other lines for future researches, aimed at complementing and enriching the present results, are shortly mentioned.

First, in the present study we limited our investigation to alpha oscillatory activity as the main general mechanism supporting attention-related shaping of cortical engagement/disengagement. In future, it will be important to associate measure of alpha band activity with measure of cortical oscillatory activity in other bands (e.g., gamma). Indeed, increase in alpha activity amplitude has been suggested to break ongoing gamma activity; therefore, investigation of the interplay between gamma and alpha activity and of how this interplay is modulated by different attention levels and different attentional components will further improve our understanding of the neural correlates of attention. However, a similar investigation will require higher electrode density and more sophisticated paradigms, for emergence of gamma rhythm.

Moreover, as previously mentioned, the present study used a limited numbers of electrodes.
This precluded both the possibility of parceling the scalp into several regions of interest, and more importantly the possibility of estimating cortical source localization via distributed source models or via equivalent dipole fitting. The interesting and novel results that have emerged from this preliminary work provide motivation to deepen the underlying neural mechanisms via high-density EEG and algorithms

of cortical source reconstruction. Moreover, via reconstruction of the activity in cerebral structures, the dynamic coupling between autonomic and cerebral signals can be investigated in a more reliable way.

5. Conclusions

In conclusion, this study examined the influence of different combinations of attentional components on EEG alpha oscillatory activity and indexes of heart rate variability. The results indicated that modulation of EEG alpha power over different regions is sensitive to the involved attentional components, being not only regulated by the coarse level of attentional demand, but also fine-tuned by the nature of the mechanisms recruited (visual, motor, cognitive) relative to the functional specification of the areas. These data provide further support to the role of alpha oscillatory activity as a neural mechanism subserving attention via allocation of cortical resources and routing of information processing in a finely and goal-oriented manner. Heart rate variability indexes appear less sensitive to different attentional components compared to alpha power, with the index of vagal tone (HF power) presenting larger modulation. Overall, the present results may have implications in applied settings such as human-factor engineering, neuroergonomics, brain-computer interfaces, but also in clinical practice and in neuroscience research investigating electroencephalographic and autonomic correlates of attention disorders.

Authors' contributions

E.M. contributed to design the study, to acquire the data, to analyze the data and interpret the results, drafted and edited the manuscript. G.R. acquired the data, contributed to analyze the data and interpret the results, and edited the manuscript. M.U. contributed to design the study, to analyze the data and interpret the results, and edited the manuscript.

Conflict of interest

The authors declare no conflict of interest.

References

1. Niedermeyer E, Lopes da Silva FH (1999) Electroencephalography: Basic Principles, Clinical Applications, and Related Fields, Philadelphia: Lippincott Williams and Wilkins.

2.

2. Pfurtscheller G, Stancak Jr A, Neuper C (1996) Event-related synchronization (ERS) in the alpha band--an electrophysiological correlate of cortical idling: a review. Int J Psychophysiol 24: 39–46.

3. Jensen O, Mazaheri A (2010) Shaping functional architecture by oscillatory alpha activity: gating by inhibition. Front Hum Neurosci 4: 186.

4. Klimesch W (2012) Alpha-band oscillations, attention, and controlled access to stored information. Trends Cogn Sci 16: 606–617.

5. Foxe JJ, Snyder AC (2011) The role of Alpha-band brain oscillations as a sensory suppression mechanism during selective attention. Front Psychol 2: 154.

6. Frey JN, Ruhnau P, Weisz N (2015) Not so different after all: The same oscillatory processes support different types of attention. Brain Res 1626: 183–197.

7. De Smedt B, Grabner RH, Studer B (2009) Oscillatory EEG correlates of arithmetic strategy use in addition and subtraction. Exp Brain Res 195: 635–642.

8. Liang Y, Liu X, Qiu L, et al. (2018) An EEG study of a confusing state induced by information insufficiency during mathematical problem-solving and reasoning. Comput Intell Neurosci 2018: 1943565.

9. Yu X, Zhang J, Xie D, et al. (2009) Relationship between scalp potential and autonomic nervous activity during a mental arithmetic task. Auton Neurosci 146: 81–86.

10. Benedek M, Schickel RJ, Jauk E, et al. (2014) Alpha power increases in right parietal cortex reflects focused internal attention. Neuropsychologia 56: 393–400.

11. Jensen O, Gelfand J, Kounios J, et al. (2002) Oscillations in the alpha band (9–12 Hz) increase with memory load during retention in a short-term memory task. Cereb Cortex 12: 877–882.

12. Tuladhar AM, ter Huurne N, Schoffelen JM, et al. (2007) Parieto-occipital sources account for the increase in alpha activity with working memory load. Hum Brain Mapp 28: 785–792.

13. Chang YC, Huang SL (2012) The influence of attention levels on psychophysiological responses. Int J Psychophysiol 86: 39–47.

14. Grabner RH, Brunner C, Leeb R, et al. (2007) Event-related EEG theta and alpha band oscillatory responses during language translation. Brain Res Bull 72: 57–65.

15. Grabner RH, De Smedt B (2011) Neurophysiological evidence for the validity of verbal strategy reports in mental arithmetic. Biol Psychol 87: 128–136.

16. Fernandez T, Harmony T, Rodriguez M, et al. (1995) EEG activation patterns during the performance of tasks involving different components of mental calculation. Electroencephalogr Clin Neurophysiol 94: 175–182.

17. Hairston WD, Whitaker KW, Ries AJ, et al. (2014) Usability of four commercially-oriented EEG systems. J Neural Eng 11: 046018.

18. Grummett TS, Leibbrandt RE, Lewis TW, et al. (2015) Measurement of neural signals from inexpensive, wireless and dry EEG systems. Physiol Meas 36: 1469–1484.

19. Mihajlovic V, Grundlehner B, Vullers R, et al. (2015) Wearable, wireless EEG solutions in daily life applications: what are we missing? IEEE J Biomed Health Inform 19: 6–21.

20. Luque-Casado A, Perales JC, Cardenas D, et al. (2016) Heart rate variability and cognitive processing: The autonomic response to task demands. Biol Psychol 113: 83–90.

21. Krakauer J, Ghez C (2000) Voluntary movement, In: Kandel ER, Schwartz JH, Jessell TM, editors, Principles of Neural Science, 4th Edition ed., New York: McGraw-Hill, 756–781.

22. Babiloni C, Vecchio F, Miriello M, et al. (2006) Visuo-spatial consciousness and parietooccipital areas: a high-resolution EEG study. Cereb Cortex 16: 37–46.

23. Gobel SM, Calabria M, Farne A, et al. (2006) Parietal rTMS distorts the mental number line: simulating 'spatial' neglect in healthy subjects. Neuropsychologia 44: 860–868.

24. Bell AJ, Sejnowski TJ (1995) An information-maximization approach to blind separation and blind deconvolution. Neural Comput 7: 1129–1159.

25. Lee TW, Girolami M, Sejnowski TJ (1999) Independent component analysis using an extended infomax algorithm for mixed subgaussian and supergaussian sources. Neural Comput 11: 417441.

26. Makeig S, Onton J (2009) ERP features and EEG dynamics: An ICA perspective, In: Kappenman ES, Luck SJ, editors, The Oxford Handbook of Event-Related Potential Components, New York: Oxford University Press, 51–86.

27. Kaufmann T, Sutterlin S, Schulz SM, et al. (2011) ARTiiFACT: a tool for heart rate artifact processing and heart rate variability analysis. Behav Res Methods 43: 1161–1170.

28. Berntson GG, Quigley KS, Jang JF, et al. (1990) An approach to artifact identification: application to heart period data. Psychophysiology 27: 586–598.

29. Babiloni C, Carducci F, Cincotti F, et al. (1999) Human movement-related potentials vs desynchronization of EEG alpha rhythm: a high-resolution EEG study. Neuroimage 10: 658665.

30. Manganotti P, Gerloff C, Toro C, et al. (1998) Task-related coherence and task-related spectral power changes during sequential finger movements. Electroencephalogr Clin Neurophysiol 109: 50–62.

31. Menon V, Rivera SM, White CD, et al. (2000) Dissociating prefrontal and parietal cortex activation during arithmetic processing. Neuroimage 12: 357–365.

32. Fournier LR, Wilson GF, Swain CR (1999) Electrophysiological, behavioral, and subjective indexes of workload when performing multiple tasks: manipulations of task difficulty and training. Int J Psychophysiol 31: 129–145.

33. Hansen AL, Johnsen BH, Thayer JF (2003) Vagal influence on working memory and attention. Int J Psychophysiol 48: 263–274.

34. Kubota Y, Sato W, Toichi M, et al. (2001) Frontal midline theta rhythm is correlated with cardiac autonomic activities during the performance of an attention demanding meditation procedure. Brain Res Cogn Brain Res 11: 281–287.

35. Duschek S, Worsching J, Reyes Del Paso GA (2015) Autonomic cardiovascular regulation and cortical tone. Clin Physiol Funct Imaging 35: 383–392.

36. Triggiani AI, Valenzano A, Del Percio C, et al. (2016) Resting state Rolandic mu rhythms are related to activity of sympathetic component of autonomic nervous system in healthy humans. Int J Psychophysiol 103: 79–87.

37. Faes L, Nollo G, Jurysta F, et al. (2014) Information dynamics of brain–heart physiological networks during sleep. New J Phys 16: 105005.

ISSN - 2373-7972

Effects of erythropoietin on bile duct ligation-induced neuro inflammation in male rats

Moazameh Golshani1, Mohsen Basiri2, Mohammad Shabani2, Iraj Aghaei3 and Majid AsadiShekaari2,*

1 Department of Anatomical Sciences, Afzalipour School of Medicine, Kerman University of Medical Sciences, Kerman, Iran

2 Neuroscience Research Center, Neuropharmacology Institute, Kerman University of Medical Sciences, Kerman, Iran

3 Neuroscience Research Center, Poursina Hospital, Guilan University of Medical Sciences, Rasht, Iran

ABSTRACT

Hepatic encephalopathy (HE) is a brain disorder as a result of liver failure. Previous studies have indicated that erythropoietin (EPO) has neuroprotective effects in different neurological diseases. This study addressed the therapeutic effect of a four-week treatment with EPO on neuronal damages in bile duct-ligated rats. Forty male Wistar rats (250–280 g) were used in the present study. The animals were randomly divided into four groups consisting of 10 animals each, including sham, sham + EPO, bile duct ligation (BDL), and BDL + EPO. EPO was intraperitoneally administered every other day (5,000 U/Kg) in the last four weeks after BDL. Biochemical and histological studies were performed to evaluate neurodegeneration. The results revealed that BDL increases the level of hepatic enzymes and total bilirubin. Furthermore, neurodegeneration was significantly increased in the BDL group compared to sham groups. EPO preserved hepatic enzymes and total bilirubin in the treated group. In addition, EPO significantly decreased the neurodegeneration in BDL + EPO compared to the BDL group. Results of this study showed that EPO has neuroprotective effects in the rat model of HE, possibly due to its anti-inflammatory and anti-oxidant properties. Complementary studies are required to clarify the exact mechanisms.

Keywords: bile duct ligation; hepatic encephalopathy; erythropoietin; astrocytes; microglia

1. Introduction

The liver plays an important role in the regulation of glycogen storage, synthesis of protein, and detoxification of various metabolites. Liver failure affects brain function and can lead to neurological and psychological changes, referred to as hepatic encephalopathy (HE). Malfunction of the liver can lead to accumulation of toxic substances such as bilirubin, urea, and ammonium in the blood [1,2]. Liver failure, hepatitis, cirrhosis, or bile duct obstruction are major factors in HE [3].

The clinical symptoms of HE depend on the rate at which liver dysfunction occurs and also the degree of metabolic disorders [4]. As the disease progresses, motor function and mental abilities become impaired. Patients show a reduced ability in terms of attention, learning, memory, and cognition, and may also suffer from motion and visual perception impairment [5,6]. These changes affect the quality of life in patients with HE and can lead to impairment in performing daily activities [7]. Hyperammonemia is a major factor in the pathogenesis of HE [8]. Toxins such as ammonia can enter the nervous system. The only way to detoxify ammonia is its conversion to glutamine, and the enzymes of this process can be found only in astrocytes. Product glutamine is transferred to neurons [9]. Increase in glutamate in the brain is characteristic of HE [10,11].

Furthermore, blocking the flow of bile from the liver to the intestine is associated with profound metabolic changes, including changes in the mitochondrial functions, reduction in fatty acid oxidation, and increases in the concentration of hydrophobic bile acids in the liver and plasma. These factors eventually cause an inflammatory response associated with the death of hepatocytes or cirrhosis [12,13]. Thus, bile flow obstruction can cause liver failure and, subsequently, HE [3]. By changing the metabolism of neurotransmitters and induction of neurotoxicity, ammonia plays a major role in the development of HE [14].

Previous scientific reports have shown that hyper-ammonia with bile duct ligation (BDL) can lead to intense activity of glial cells in the cerebellum and some areas of the hippocampus [15]. Activation of microglia is associated with the release of inflammatory factors and an increase in the concentrations of pro-inflammatory cytokines in the brain, followed by the severe swelling of astrocytes and brain edema which refers to HE [16,17]. Different agents such as EPO [18] and pioglitazone [19] are effective against neuronal impairments observed in BDL rats. Interestingly, macrophages expressing EPO receptors and EPO have been reported to suppress inflammatory macrophage activation [20]. EPO is a neuroprotective agent acting by the inhibition of neuronal apoptosis and reduction of neuroinflammation [21].

In our previous studies, we found that BDL rats manifest motor and spatial learning and memory impairments, and chronic treatment with EPO alleviates these impairments [18]. In the present study, the effect of EPO on neuronal degeneration and astrocyte and microglia activity was evaluated in the CA1 subfield of the hippocampus and cerebellum of male rats following common BDL.

2. Materials and methods

In the present study, male Wistar rats (n = 40, 2 months old, 250–280 g) were used. The handling and care of the animals were conducted according to the National Guidelines on Animal Care and was approved by the Ethics Committee of the Kerman University of Medical Sciences (Ethics Code: IR.KMU.REC.1396.1140.). Animals were kept under standard conditions; room temperature was controlled (20 ± 2 ℃) and a 12h on-off light-dark cycle was maintained with free access to water and food. The rats were randomly divided into four groups consisting of 10 animals in each group (sham surgery, sham surgery + EPO, BDL surgery, and BDL surgery + EPO). EPO was prepared from Pooyesh Darou Product Company and intraperitoneally administered every other day (5,000 U/Kg) [i.p.] in the final four weeks after BDL [18].

Sham and BDL surgery groups received saline intraperitoneally in the same volume and based on the time schedule considered for EPO groups. All experimental studies were performed in a blind manner.

2.1. BDL procedure

Rats were anaesthetized (ketamine 90 mg/kg, xylazine 12 mg/kg, i.p.). A middle abdominal incision was performed. Then, after cutting the fascia and muscles, the common bile duct was ligated with a 4–0 silk suture at two points posterior to the hilum of the liver and anterior to the pancreas. The abdominal incision was closed in two layers. In sham animals, the common bile duct was manipulated but not ligated. All animals were maintained for six weeks following the surgery [4,22]. The mortality rate was 20% in the BDL group and 5% in the BDL surgery + EPO, and new animals were replaced.

2.2. Biochemical and cytological parameters

Animals were sacrificed under deep anesthesia at the end of the sixth week of surgery and blood samples were collected by carotid bleeding. The following parameters were biochemically assayed in the plasma separated from blood samples: total bilirubin (Sigma, MAK126), alkaline phosphatase (ALP) (Sigma, APF), Aspartate transaminase (AST) (Sigma, MAK055) and hepatic albumin (Sigma, MAK124) using a commercially available kit. In addition, cytological parameters, consisting of red blood cells (RBCs) and hemoglobin were evaluated [23,24].

2.3. Tissue preparation

Animals were sacrificed under deep anesthesia six weeks after BDL and their brain was removed and dissected into hippocampal and cerebellum blocks. The brains were fixed in a 10% formalin solution for

48 h and processed for histological and immunohistochemistry (IHC) analysis.

2.4. Nissl staining

To assess the morphology of hippocampus and cerebellum neurons, the Nissl staining method was employed. Coronal sections (8 μm) were cut from the hippocampus and cerebellum using a rotary microtome. Briefly, sections were deparaffinized through xylene and alcohols into tap water, stained in 0.1% cresyl violet solution for 5 min, dehydrated in 100% alcohol, and then cleared in xylene. Pyramidal neurons of the CA1 sector of the hippocampus and Purkinje cells of the cerebellum were manually counted in three microscopic fields (0.107 mm2; 89.82 × 120.70 μm) of the Nissl stained sections from the hippocampus and cerebellum. Results are expressed as the average number of cells/0.1 mm2.

2.5. Immunohistochemistry

Astrocyte glial fibrillary acidic protein (GFAP) and microglia (CD11) were counted in order to evaluate astrocyte and microglial activity. The sections were immunostained using the polyclonal primary antibody for GFAP (1:400) (PA1239) or CD11 (1:500) (DB Biotech). The sections were deparaffinized in xylene, hydrated through a graded ethanol series, and washed in running water. After antigen retrieval, the sections were incubated with rabbit primary antibody GFAP [25] and mouse primary antibody CD11 [26] overnight at 4 °C. Afterwards, the sections were rinsed for 10 min with phosphate buffer solution (PBS) and incubated with horseradish peroxidase (HRP)-conjugated anti-rabbit and anti-mouse antibodies (Santa Cruz Biotechnology, Inc., USA) at the dilution of 1:200 for 1 h at room temperature. After washing in PBS, peroxidase activity was detected with 3, 3-diaminobenzidine (DAB, Abcam, UK) as the chromogenic substrate. The sections were counterstained with hematoxylin (Sigma-Aldrich, USA), dehydrated in an increasing alcohol series, cleared in xylene, and finally mounted on Entellan® (Merck, Germany). Astrocytes showing GFAP and CD11+ cells were manually counted in three microscopic fields (0.107 mm2; 89.82 × 120.70 μm) of the immunohistochemically stained sections from the cerebellum and hippocampus. Results are expressed as the average number of cells/0.1 mm2.

2.6. Statistical analyses

All statistical analyses were performed using SPSS (v.22). All data were calculated for normality using the Kolmogorov-Smirnov test. Results were normally distributed ($p < 0.05$ in K-S test), and therefore expressed as the mean ± SEM and analyzed using one-way ANOVA. Tukey's post-hoc analysis was used for the analysis of data, and $p < 0.05$ was considered as the significance level.

3. Results

3.1. Effects of BDL and EPO on biochemical and cytological parameters

The levels of biochemical and cytological parameters were elevated as a result of BDL surgery after six weeks. Based on our data, BDL induction resulted in a significant increase ($p < 0.05$) in ALP and ALT levels and the administration of EPO counteracted these effects. Total bilirubin levels were elevated in BDL animals and were not affected by EPO administration, either in sham or in BDL animals. EPO administration increased the number of RBCs in sham and BDL groups. There was no significant change in the level of hemoglobin across groups. The level of albumin markedly increased in the BDL rats with the EPO treatment compared to BDL (Table 1).

3.2. Effect of BDL and EPO on neuronal degeneration

Nissl staining was performed to determine neuronal degeneration. Results showed that BDL significantly increased the number of degenerated neurons in the hippocampus (Figure 1A) and cerebellum (Figure 1B) compared to the shams group. Treatment with EPO significantly decreased BDL-induced neurodegeneration.

Table 1. The effects of BDL and EPO treatment on hepatic enzymes, albumin, bilirubin total, hemoglobin, and RBCs.

Groups	AST (U/l)	ALP (U/l)	Albumin (g/dl)	Bilirubin total (mg/dl)	RBC (number × 106 ul)	Hb (g/dl)
Sham	598 ± 88.7	416 ± 7.23	3.40 ± 0.3	0.4 ± 0.1	5.53 ± 0.07	11.5 ± 0.3
BDL	1138 ± 24.99*	613 ± 5.69*	1.90 ± 0.06*	8.5 ± 0.26*	4.5 ± 0.21	10.6 ± 0.33
Sham + EPO	481 ± 5.11$	329 ± 3.79$	3.97 ± 0.08$	0.76 ± 0.02$	9.66 ± 0.27$	13.7 ± 0.31
BDL + EPO	845 ± 8.41#	531 ± 4.77#	3.06 ± 0.04#	9.4 ± 0.29	6.5 ± 0.16	11.8 ± 0.07

Note: BDL significantly increased the level of AST and ALP. The level of total bilirubin was significantly increased in BDL rats. Albumin level was decreased in BDL and BDL+EPO rats. Moreover, EPO treatment reduced AST and ALP levels. BDL did not significantly change the RBC parameters, although EPO increased these parameters. *$p < 0.05$, compared with the sham; $ and # $p < 0.05$, compared with the BDL.

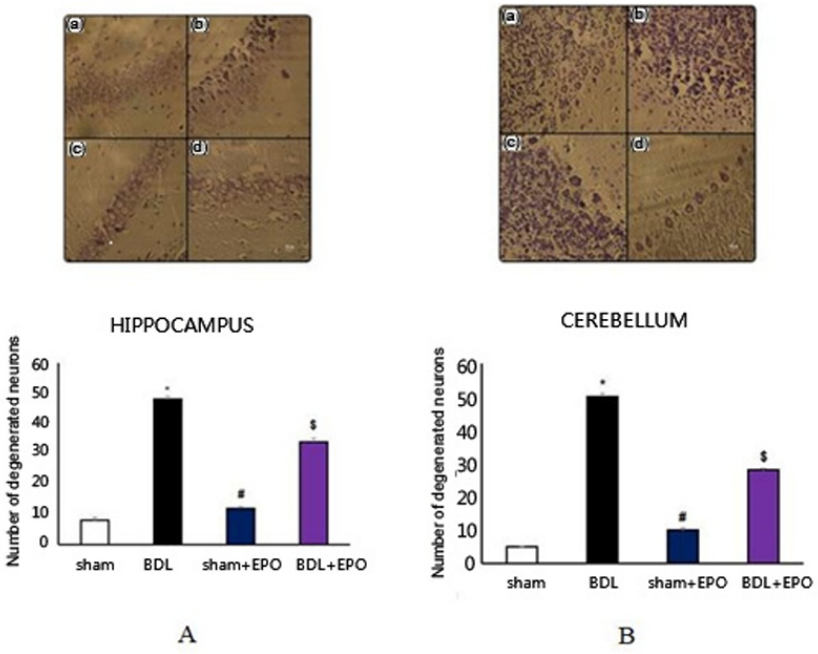

Figure 1. The effects of BDL and EPO treatment on neuronal injury induced by BDL in male rats. Representative photomicrographs showing cerebellar architecture (A) and hippocampus (B) in male rats in different groups: (a) sham, (b) BDL, (c) sham + EPO, (d) BDL + EPO. BDL induced insults to cerebellar Purkinje and hippocampal pyramidal neurons and the administration of EPO ameliorated the detrimental effects in treated animals. The figure shows the quantitative analysis of and hippocampal pyramidal neurons cerebellar Purkinje in different groups. Data are the mean ± SEM. *$p < 0.001$ compared with the sham group; # and \$ $p < 0.001$ compared with BDL (one-way ANOVA with Tukey's post-hoc test for all comparisons).

3.3. Effect of BDL and EPO on glial cells

Differences in the number of GFAP+ and CD11+ cells between the different groups in the hippocampus and cerebellum were analyzed using one-way ANOVA. Results demonstrated that the number of GFAP+ cells in the BDL group was significantly higher than the sham and sham + EPO groups ($p < 0.001$) in the hippocampus (Figure 2A) and cerebellum (Figure 2B), whereas EPO treatment significantly decreased cell number in the treated group ($p < 0.01$).

In addition, the data demonstrated that the number of CD11+ cells was significantly higher in the BDL than sham and sham + EPO ($p < 0.001$) groups, whereas cell number was significantly decreased in the EPO treated group ($p < 0.01$, Figure 3A and 3B).

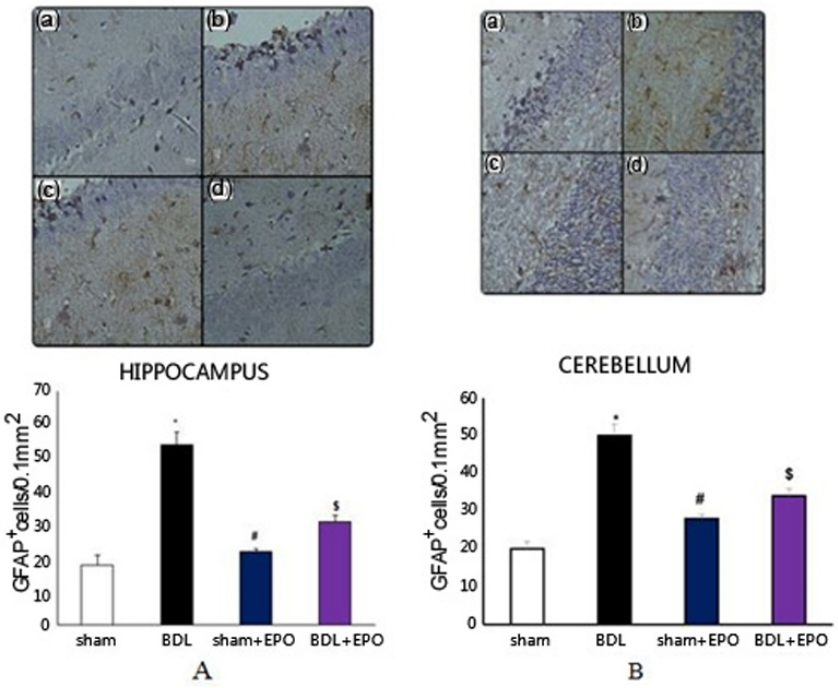

Figure 2. The effect of BDL and EPO treatment on the number of GFAP+ cells in the hippocampus (A) and cerebellum (B) of rats. Representative photomicrographs showing GFAP+ cell morphology after staining using antibodies against GFAP in different groups of rats: (a) sham, (b) BDL, (c) sham + EPO, (d) BDL + EPO. Nuclei were stained with hematoxylin (blue). Magnification 400×. The graph shows the quantitative analysis of GFAP+ cells in the hippocampus and cerebellum of rats in different groups. Data are the mean ± SEM. *$p < 0.001$ compared with the sham group; # and $ ($p < 0.001$ and 0.1, respectively) compared with BDL (one-way ANOVA with Tukey's post-hoc test for all comparisons).

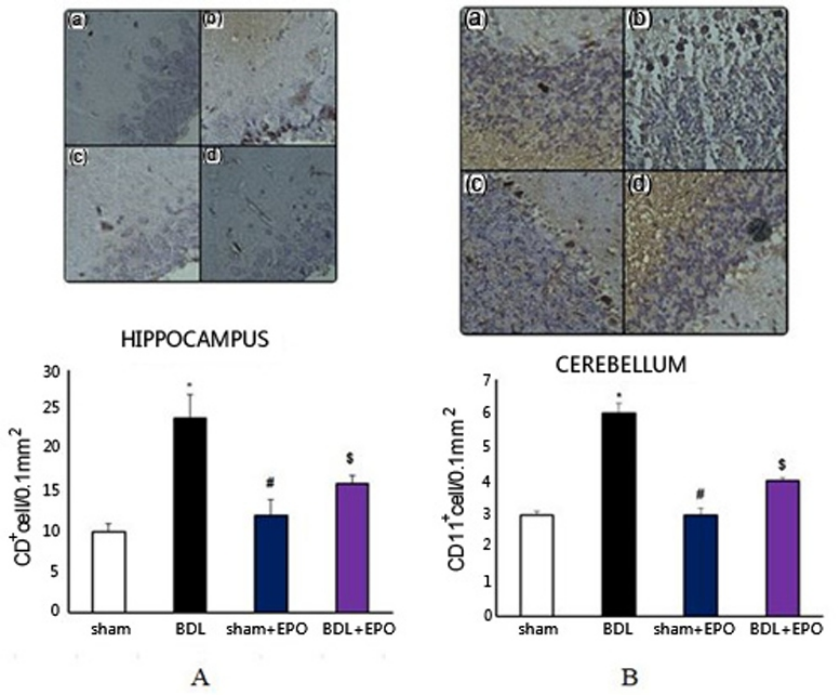

Figure 3. The effect of BDL and EPO treatment on the densitometry of CD11+ cells in the (A) hippocampus and cerebellum (B) of rats. Representative photomicrographs showing CD11+ cell morphology after staining using antibodies against CD11 in different groups of rats: (a) sham, (b) BDL, (c) sham + EPO, (d) BDL + EPO. Nuclei were stained with hematoxylin (blue). Magnification 400×. The graph shows the quantitative analysis of CD11+ cells of hippocampus and cerebellum in different groups. Data are the mean ± SEM. *$p < 0.01$ compared with the sham group; # and $ $p < 0.01$ compared with BDL (one-way ANOVA with Tukey's post-hoc test for all comparisons).

4. Discussion

Previous studies have demonstrated deficits in motor and cognitive in both clinical and animal experiments of HE following BDL [18,27,28]. Previously, the possible effect of EPO as a potent neuroprotective agent on motor and cognitive impairments induced by HE were also identified. In the present study, the effects of EPO on the neuronal degeneration and astrocyte and microglia activity of male rats following BDL were investigated. Deficits in liver function and neuronal degeneration were observed in rats following BDL as an animal model of HE. EPO had a neuroprotective function against hepatic enzyme impairments and neurodegeneration induced by BDL. Although the exact mechanisms of impairments are not yet clear, neural apoptosis, oxidative stress, and excitotoxicity have been proposed to underlie these impairments [1]. Increased levels of free radicals have been observed in the brain of BDL rats [29]. Therefore, finding strategies to decrease these oxidative changes may help reduce the impairments observed in HE.

EPO is responsible for RBC production stimulation in the bone marrow. It has been demonstrated that EPO can be a potent neuroprotective agent [1]. BDL is known to induce neural damage through oxidative stress and metabolic imbalance [29]. Therefore, it appears that EPO may exert its effect on BDL-induced impairments through these pathways.

In agreement with a previous study, BDL induced a significant increase in the bilirubin level of BDL rats [30], and EPO did not alter this biochemical change in the male rats. This may imply that EPO protects neurons from other pathways [31]. Additionally, as a result of the present study, BDL-induction resulted in a decrease in albumin, and EPO administration reversed the effect of BDL. Thus, EPO may protect neurons through its albumin increasing activity.

Albumin provides more than 50% of the total antioxidant of the plasma. The activity is attributed to the abundant reduced sulfhydryl groups of albumin that can scavenge a variety of free radicals such as nitric

oxide and hypochlorous acid. On the other hand, albumin can bind to unconjugated bilirubin, a potent antioxidant. It is believed that this antioxidant activity is usually assumed to be the mechanism responsible for the potent inverse correlation between plasma unconjugated bilirubin concentration and mortality of many diseases [32]. In the present study, the data demonstrated that EPO ameliorates biochemical impairments induced by BDL. Caillaud et al. showed that EPO reduces the systematic oxidative stress in the treated rats [33]. Consequently, the possible mechanism of action for EPO may be through its antioxidant properties. Previous studies have shown that BDL can lead to neuronal degeneration and activation of astrocytes and microglia in the hippocampus and cerebellum [21,34–36]. Several studies have suggested that EPO, as an internal mediator, has significant neuroprotective effects in various disorders of the central nervous system (CNS) [37]. It possibly acts as a neuroprotective agent in the treatment of neurodegenerative diseases by modulating inflammatory factors [38–40]. Bond et al. reported that, through the reduction of reactive oxygen species (ROS) levels, EPO inhibits neuroinflammation and neuronal death [21].

In this study, the results revealed an increase in GFAP+ and CD11+ cells in the cerebellum and hippocampus following BDL, and the number of these cells showed more astrocytes compared to microglia cells in these areas. Microglia cells are known as the first line of defense against CNS disorders and injuries, including stroke, brain injury, and spinal cord injury [41]. There is extensive evidence that microglia cells have an important role in CNS homeostasis and its related damage. Following damage, microglia cells quickly migrate to the lesion site and prevent long-term lesion progress [41]. Activation of microglial cells is an important part of neuroinflammation, widely discussed in HE. Astrocytes are known as key cells in brain damage due to acute liver disease, but there is evidence that microglia cells are equally involved in neuroinflammation as a result of acute liver disease [42].

Jayakumar et al. showed that hyperammonemia following HE leads to microglia (mainly in the cerebellum) and brain endothelial cell activation that is associated with the production and release of inflammatory factors as a result of which astrocytic swelling and cerebral edema occurs [16]. Bond et al. showed that, through decreasing the level of ROS and reactive nitrogen species, EPO limits the microglia and astrocytes infiltration. On the other hand, EPO can maintain the health of endothelial cells of the blood-brain barrier [21].

5. Conclusion

In conclusion, our results demonstrated that EPO administration can reduce cholestasis-induced liver dysfunction. It also reduces neurodegeneration in the hippocampus and cerebellum following BDL.

Additionally, EPO modulates the number of GFAP+ and CD11+ cells in BDL groups. These effects are probably related to the potential anti-oxidant and anti-inflammatory effect of EPO. However, further studies are needed to prove this hypothesis.

Acknowledgments

This research was supported by the Neuroscience Research Center of Kerman University of Medical Sciences. The data presented in this scientific paper are taken from Moazameh Golshani's MSc thesis.

Conflict of interest

The authors declare no conflict of interest.

References

1. Felipo V (2013) Hepatic encephalopathy: effects of liver failure on brain function. Nat Rev Neurosci 14: 851–858.

2. Olde Damink SW, Jalan R, Dejong CH (2009) Interorgan ammonia trafficking in liver disease. Metab Brain Dis 24: 169–181.

3. Butterworth RF, Norenberg MD, Felipo V, et al. (2009) Experimental models of hepatic encephalopathy: ISHEN guidelines. Liver Int 29: 783–788.

4. Leke R, Oliveira DL, Forgiarini LF, et al. (2013) Impairment of short term memory in rats with hepatic encephalopathy due to bile duct ligation. Metab Brain Dis 28: 187–192.

5. Weissenborn K, Giewekemeyer K, Heidenreich S, et al. (2005) Attention, memory, and cognitive function in hepatic encephalopathy. Metab Brain Dis 20: 359–367.

6. Ferenci P, Lockwood A, Mullen K, et al. (2002) Hepatic encephalopathy--definition, nomenclature, diagnosis, and quantification: final report of the working party at the 11th World Congresses of Gastroenterology, Vienna, 1998. Hepatology 35: 716–721.

7. Patel A, Wade JB, Thacker LR, et al. (2014) 991 Brain Reserve Modulates Health-Related Quality of Life in Patients With Cirrhosis Independent of Covert Hepatic Encephalopathy and MELD Score. Gastroenterology 146: S–932.

8. Rose CF (2012) Ammonia-lowering strategies for the treatment of hepatic encephalopathy. Clin Pharmacol Ther 92: 321–331.

9. Savlan I, Liakina V, Valantinas J (2014) Concise review of current concepts on nomenclature and pathophysiology of hepatic encephalopathy. Medicina (Kaunas) 50: 75–81.

10. Rama Rao KV, Jayakumar AR, Norenberg MD (2012) Glutamine in the pathogenesis of acute hepatic encephalopathy. Neurochem Int 61: 575–580.

11. Rothman DL, De Feyter HM, Maciejewski PK, et al. (2012) Is there in vivo evidence for amino acid shuttles carrying ammonia from neurons to astrocytes? Neurochem Res 37: 2597–2612.

12. Jover R, Rodrigo R, Felipo V, et al. (2006) Brain edema and inflammatory activation in bile duct ligated rats with diet-induced hyperammonemia: A model of hepatic encephalopathy in cirrhosis. Hepatology 43: 1257–1266.

13. Sheen JM, Huang LT, Hsieh CS, et al. (2010) Bile duct ligation in developing rats: temporal progression of liver, kidney, and brain damage. J Pediatr Surg 45: 1650–1658.

14. Aldridge DR, Tranah EJ, Shawcross DL (2015) Pathogenesis of hepatic encephalopathy: role of ammonia and systemic inflammation. J Clin Exp Hepatol 5: S7–S20.

15. Rodrigo R, Cauli O, Gomez-Pinedo U, et al. (2010) Hyperammonemia induces neuroinflammation that contributes to cognitive impairment in rats with hepatic encephalopathy. Gastroenterology 139: 675–684.

16. Jayakumar AR, Rama Rao KV, Norenberg MD (2015) Neuroinflammation in hepatic encephalopathy: mechanistic aspects. J Clin Exp Hepatol 5: S21–28.

17. Butterworth RF (2012) Reprint of: Neuroinflammation in acute liver failure: Mechanisms and novel therapeutic targets. Neurochem Int 60: 715–722.

18. Aghaei I, Nazeri M, Shabani M, et al. (2015) Erythropoietin ameliorates the motor and cognitive function impairments in a rat model of hepatic cirrhosis. Metab Brain Dis 30: 197–204.

19. Aghaei I, Shabani M, Doustar N, et al. (2014) Peroxisome proliferator-activated receptorgamma activation attenuates motor and cognition impairments induced by bile duct ligation in a rat model of hepatic cirrhosis. Pharmacol Biochem Behav 120: 133–139.

20. Nairz M, Schroll A, Moschen AR, et al. (2011) Erythropoietin contrastingly affects bacterial infection and experimental colitis by inhibiting nuclear factor-kappaB-inducible immune pathways. Immunity 34: 61–74.

21. Bond WS, Rex TS (2014) Evidence that erythropoietin modulates neuroinflammation through differential action on neurons, astrocytes, and microglia. Front Immunol 5: 523.

22. Aghaei I, Hajali V, Dehpour A, et al. (2016) Alterations in the intrinsic electrophysiological properties of Purkinje neurons in a rat model of hepatic encephalopathy: Relative preventing effect of PPARgamma agonist. Brain Res Bull 121: 16–25.

23. Shabani M, Ebrahimpoor F, Firouzjaei MA, et al. (2019) Modulation of sphingosine-1phosphate receptor by FTY720 contributes in improvement of hepatic encephalopathy induced by bile duct ligation. Brain Res Bull 146: 253–269.

24. Tahamtan M, Aghaei I, Pooladvand V, et al. (2017) Characterization of the CA1 pyramidal neurons in rat model of hepatic cirrhosis: insights into their electrophysiological properties. Metab Brain Dis 32: 881–889.

25. Onoda A, Takeda K, Umezawa M (2017) Dose-dependent induction of astrocyte activation and reactive astrogliosis in mouse brain following maternal exposure to carbon black nanoparticle. Part Fibre Toxicol 14: 4.

26. Matsui H, Ohgomori T, Natori T, et al. (2013) Keratan sulfate expression in microglia is diminished in the spinal cord in experimental autoimmune neuritis. Cell Death Dis 4: e946.

27. Javadi-Paydar M, Ghiassy B, Ebadian S, et al. (2013) Nitric oxide mediates the beneficial effect of chronic naltrexone on cholestasis-induced memory impairment in male rats. Behav Pharmacol 24: 195–206.

28. Nasehi M, Piri M, Abbolhasani K, et al. (2013) Involvement of opioidergic and nitrergic systems in memory acquisition and exploratory behaviors in cholestatic mice. Behav Pharmacol 24: 180–194.

29. Butterworth RF (2011) Hepatic encephalopathy: a central neuroinflammatory disorder? Hepatology 53: 1372–1376.

30. Huang LT, Tiao MM, Tain YL, et al. (2009) Melatonin ameliorates bile duct ligation-induced systemic oxidative stress and spatial memory deficits in developing rats. Pediatr Res 65: 176180.

31. Brines M, Cerami A (2005) Emerging biological roles for erythropoietin in the nervous system. Nat Rev Neurosci 6: 484–494.

32. Levitt DG, Levitt MD (2016) Human serum albumin homeostasis: a new look at the roles of synthesis, catabolism, renal and gastrointestinal excretion, and the clinical value of serum albumin measurements. Int J Gen Med 9: 229–255.

33. Caillaud C, Mechta M, Ainge H, et al. (2015) Chronic erythropoietin treatment improves dietinduced glucose intolerance in rats. J Endocrinol 225: 77–88.

34. Dhanda S, Sandhir R (2015) Role of dopaminergic and serotonergic neurotransmitters in behavioral alterations observed in rodent model of hepatic encephalopathy. Behav Brain Res 286: 222–235.

35. Su YY, Yang GF, Lu GM, et al. (2015) PET and MR imaging of neuroinflammation in hepatic encephalopathy. Metab Brain Dis 30: 31–45.

36. Chen JR, Wang BN, Tseng GF, et al. (2014) Morphological changes of cortical pyramidal neurons in hepatic encephalopathy. BMC Neurosci 15: 15.

37. Ponce LL, Navarro JC, Ahmed O, et al. (2013) Erythropoietin neuroprotection with traumatic brain injury. Pathophysiology 20: 31–38.

38. Wenker SD, Chamorro ME, Vittori DC, et al. (2013) Protective action of erythropoietin on neuronal damage induced by activated microglia. FEBS J 280: 1630–1642.

39. McPherson RJ, Juul SE (2008) Recent trends in erythropoietin-mediated neuroprotection. Int J Dev Neurosci 26: 103–111.

40. Mofidi A, Bader A, Pavlica S (2011) The use of erythropoietin and its derivatives to treat spinal cord injury. Mini Rev Med Chem 11: 763–770.

41. Hu X, Liou AK, Leak RK, et al. (2014) Neurobiology of microglial action in CNS injuries: receptor-mediated signaling mechanisms and functional roles. Prog Neurobiol 119–120: 60–84. 42. Wright G, Swain M, Annane D, et al. (2016) Neuroinflammation in liver disease: sessional talks from ISHEN. Metab Brain Dis 31: 1339–1354.

ISSN - 2373-7972

Comparing methods for scaling shape similarity

Ernest Greene*
Laboratory for Neurometric Research, Department of Psychology, University of Southern California, Los Angeles, California, USA

1. Introduction

It is useful to evaluate alternative methods for quantifying shape attributes to see which best predicts human judgments of shape similarity. Any insights that might be garnered would contribute to our understanding of visual mechanisms, and would also have potential applications in artificial intelligence—more specifically in machine vision. This brief commentary provides a recap of recent work from my laboratory that was directed to the attention of the artificial intelligence community [1] but which should also be of interest to those who study biological vision. It compared two computational methods for scaling similarity of two-dimensional shapes, followed by an experiment that determined the degree to which the scale values predicted human judgments of similarity. The results are at odds with a classic concept that proximity of neighboring contours is a prime factor in the perception of shape similarity.

Procrustes analysis was one of the methods used to assess shape similarity. Procrustes analysis is a statistical method for comparing shape pairs that normalizes distances of boundary markers relative to their centroids, centers the shapes on their centroids, and then derives the minimum Euclidean distance among all pairs of markers. It has strong mathematical roots [2–5], and has been applied in various engineering and scientific fields, including classification of rock formations [6], and classification of facial features [7]. In biology it is known as geometric morphometrics [8,9]. A comprehensive overview of alternative implementations is provided by Dryden & Mardia [10].

For comparing 2D shapes formed as outline boundaries, one must discretize the perimeter to provide an equal number of location markers, as illustrated in Figure 1. The analysis requires an iterative assessment of spans between marker pairs at all perimeter locations. One arbitrarily chooses a marker from each shape, assesses the span between them, then steps to the next adjacent pair to assess that span, then the next, and so forth until all pairs have been evaluated. The mean of these spans is calculated, and that becomes a candidate similarity value. Passing through all of the pairs is not sufficient, however, for the starting pair that were chosen might not provide the minimum mean value. So one returns to the

starting point on one shape, pairs with the marker position on the other shape that is one step away from what was previously used, and repeats the loop around the boundary to derive another candidate mean value. This iterative process continues until all combinations of marker locations have been measured, after which the lowest mean value is chosen as reflecting the degree to which the two shapes are similar. A comprehensive Procrustes analysis could include adjustments for rotation and size, but here those steps were not applied because the size and orientation of target shapes remained unaltered for human judgments of similarity.

The second method for scaling similarity is based on the novel concept that shape encoding has evolutionary roots in motion processing by the retina or optic tectum. Motion of the object or eye can register the encounter of contours in the image, and waves within a neural network might be used to register stationary contours. One can model the concept with polling waves that pass across a shape, providing a successive count of the number of boundary markers that are encountered. These counts provide bin values of a histogram.

Greene & Patel [11] used polling waves that passed across each shape in the horizontal and vertical directions, and combined these in tandem into a single histogram. To adjust for differences in shape size, the raw histograms were re-binned and normalized to provide a 20-bin "summary histogram" for each shape. Similarity values were derived using a sum of squared differences calculation for each of the summary histograms. The scan registration and comparison steps are illustrated in the lower panels of Figure 1.

An inventory of 480 unknown shapes were used for scaling of similarity, as this avoids complications that might be provided from long-term memory. Each shape consisted of an outline boundary formed by a continuous string of discrete dots (see Figure 1). Procrustes similarity values were derived from the pairs that were approximately the same size (then adjusted to have equal dot counts), and these were ranked and appear as the purple-colored sigmoid in Figure 2A. That panel also plots the scan similarity value that corresponds to each of the ranked Procrustes values, which appear as the widely scattered pattern of green tokens. Panel B shows the reverse, wherein the green sigmoid provides the ranked scan-similarity values and the Procrustes values are widely scattered purple tokens. A lack of correspondence for the two similarity measures is suggested by the plots themselves, and this was confirmed by finding the correlation of the ranked values to be −0.14. This small negative correlation indicates that the two methods are assessing different shape attributes.

An assessment of the degree to which the scale values predicted human judgments of similarity was

conducted using a match-recognition protocol [12]. The basic task uses an inventory of unknown shapes, each formed as a continuous string of discrete dots, like the examples shown in Figure 1. Each shape is briefly displayed as a target only once. This is quickly followed by display of a comparison shape that is a low-density version of the target or a low-density version of a different shape. The respondent judges whether the comparison display matches the target, or not, by saying "same" or "different."

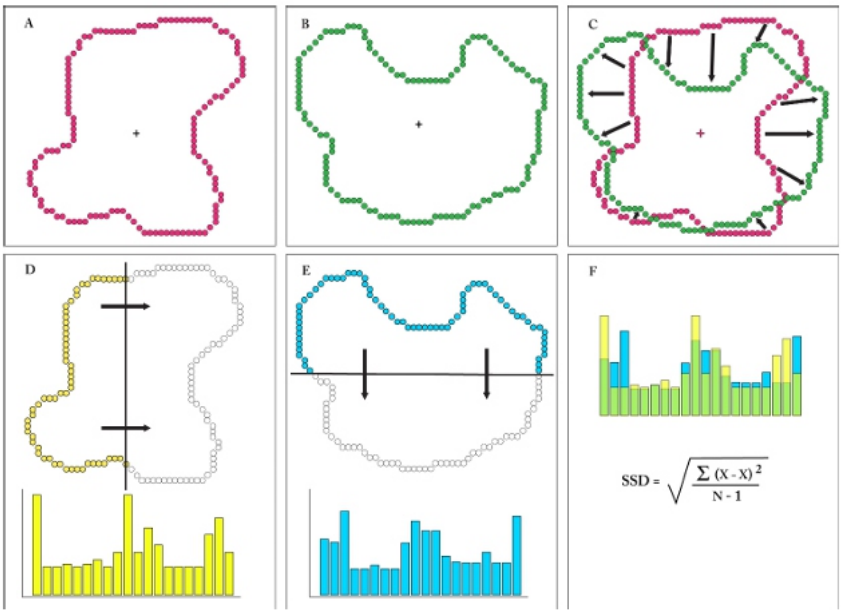

Figure 1. The upper panels of the figure illustrate the Procrustes method. Panels A and B show two shapes that have an equal number of boundary markers (dots). The centroid for each shape is shown with a plus sign. Panel C shows the shapes superimposed, and centered on the centroids. The arrows represent spans between the boundary markers, as required by the Precrustes method. The mean across all corresponding markers around the boundary would be calculated, and this process repeated with stepped pairing to determine the minimum mean span. This value provides an assessment of the similarity of the two shapes, the smaller the value, the greater the similarity. Panels D and E illustrate the scan method for summarizing the two shapes. Each shape is scanned with both a horizontal and vertical sweep by polling waves, though in each panel only a partial scan in one direction is illustrated. A polling wave provides a successive count of the number of boundary markers being encountered, and these values are further processed to provide a histogram that serves as the shape summary (as shown below each shape). Panel F shows comparison of the shape summaries using a sum-of-squared differences calculation, the resulting value providing a measure of shape similarity. A smaller value is provided by greater overlap of the histograms (green), with a smaller value indicating greater similarity of the shape summaries.

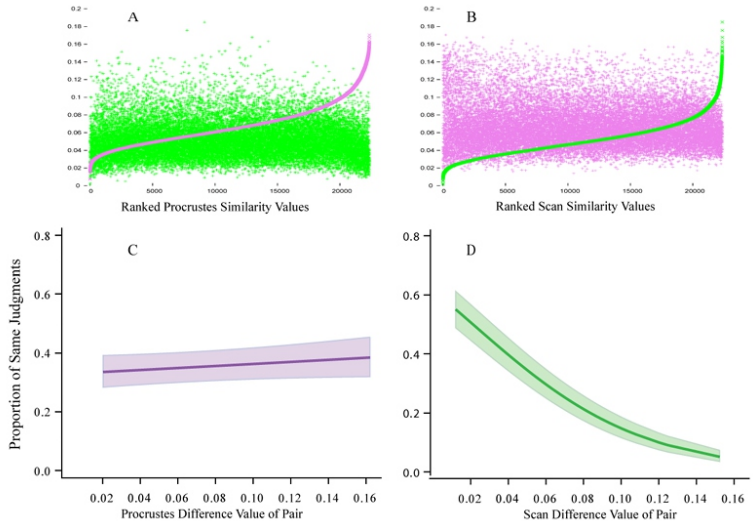

Figure 2. In panel A the pairs have been ranked according to the size of the Procrustes similarity values, wherein the sigmoid function (purple) provides a Procrustes scale of shape similarity. The corresponding scan similarity for each of the pairs is shown with green tokens. Panel B shows the reverse. The size of a given Procrustes value appears to be unrelated to the size of the corresponding scan value, and this was confirmed by a lack of correlation (see text). Panels C and D show binomial regression models and confidence intervals for perceptual judgments in a match-recognition task. The size of the Procrustes values did not predict the probability that the shape pairs would be seen as similar, but the scan values provided significant prediction of similarity judgments.

The use of low-density comparison shapes is required to prevent perfect performance, which would the outcome if the full complement of boundary markers were provided by the comparison displays. The judgment can be described as "match recognition" though it is clear that the lowdensity version of the target is not identical to the target. It is more accurate to say that the respondent is judging the similarity of the shapes that were provided by the target and comparison displays, and that works well for assessing which of the similarity scales provides the best prediction of human shape judgment. This can be done by assessing whether the size of the scale value predicts the probability that respondents will judge a given pair combination to be the "same" or see them as "different." So here the comparison shape is never a low-density version of the target, per se, but the degree to which a respondent judges a pair member as being the same as the target reflects the similarity of the two shapes.

A random sample of 320 pairs was chosen from the ranked combinations, and 20 respondents judged whether a given pair displayed the same shape. The Procrustes and scan methods had provided similarity scale values for each of the pairs, so the question was how well those values predicted the probability of "same" judgments. This was assessed with binomial regressions, which are shown in the lower panels of

Figure 2. It is clear from panel C that the Procrustes scale values do not predict the probability that the pairs would be seen as similar, and the correlation of the two measures was essentially zero. The binomial regression for the scan-similarity values against probability of same judgments (panel D) was significant at $p < 0.0001$, and the correlation of the two values was 0.40.

It is somewhat surprising to see that the Procrustes method does not predict human perception of similarity. The concept that similarity would be determined by the relative proximity of adjacent locations around the boundary is intuitively appealing, and the calculation of spans provides an appropriate implementation of that concept. The critical failure may be that the method is intrinsically local. Biological vision may draw more heavily on the global relationships that are present in a given shape, this being the view advocated by Gestalt theorists. The scan method converts the relative positioning of boundary markers into bin counts, wherein the markers at various locations along the boundary are included at different locations within the summary histogram. A given bin reflects not only how many boundary markers were encountered by a scan wave, but also the location of that portion of the boundary relative to the full span of the shape. Finding that the scan-similarity measures correlate with human judgments of similarity provides support for the proposition that 2D shapes are summarized using scan waves that convert the shape into a 1D message that can be more readily transmitted and stored as an information packet.

Scan encoding is based on movement of the polling wave. A number of laboratories have proposed that motion is involved in the encoding of contrast information, especially that provided by contours. Greene [13] suggested that spreading waves generated by retinal polyaxonal amacrine cells may be involved in the encoding of shape information. Gollisch & Meister [14] proposed that retinal ganglion cells are synchronously activated by local contrast at the end of saccadic eye movements. Ahissari & Arieli [15] as well as Rucci & Victor [16] argue that the drift that occurs between fixations can contribute to contour detection.

There are numerous alternative ways that scan waves might be used to encode boundary marker locations, and the findings described above do not provide firm evidence that the visual system makes use of scan encoding. However, new concepts for shape encoding are needed [17], and these results suggest that the scan concept should be further investigated.

Acknowledgment

This work was supported by the Quest for Truth Foundation.

Conflict of interest

The author declares no conflict of interest.

References

1. Greene E, Morrison J (2018) Computational scaling of shape similarity that has potential for neuromorphic implementation. IEEE Access 6: 38294–38302.

2. Kandell DG (1981) The statistics of shape. In: Barnett V ed, Interpreting Multivariate Data, New York: Wiley & Sons, 75–80.

3. Kandell DG (1984) Shape-manifolds, Procrustean metrics and complex projective spaces. Bull Lond Math Soc 16: 81–121.

4. Kandell DG (1985) Exact distributions for shapes of random triangles in convex sets. Adv App Prob 17: 308–329.

5. Goodall C (1991) Procrustes methods in the statistical analysis of shape. J Royal Stat Soc B 53: 285–339.

6. Vermeesch P, Garzanti E (2015) Making geological sense of "big data" in sedimentary provenance. Chem Geol 409: 20–27.

7. Mitteroecker P, Gunz P, Windhager S, et al. (2013) A brief review of shape, form, and allometry in geometric morphometrics, with applications to human facial morphology. Hystrix Ital J Mammal 24: 59–66.

8. O'Higgins P (2000) The study of morphological variation in the hominid fossil record: biology, landmarks and geometry. J Anat 197: 203–220.

9. Slice DE (2007) Geometric morphometrics. Ann Rev Anthropol 36: 261–281.

10. Dryden IL, Mardia KV (2016) Statistical Shape Analysis (2nd Ed), United Kingdom: Wiley & Sons.

11. Greene E, Petel Y (2018) Scan transcription of two-dimensional shapes as an alternative neuromorphic concept. Trends Artific Intell 1: 27–33.

12. Greene E, Hautus MJ (2017) Demonstrating invariant encoding of shapes using a matching judgment protocol. AIMS Neurosci 4: 120–147.

13. Greene E (2007) Retinal encoding of ultrabrief shape recognition cues. PLoS One 2: e871.

14. Gollisch T, Meister M (2008) Rapid neural coding in the retina with relative spike latencies. Science 319: 1108–1111.

15. Ahissar E, Arieli A (2012) Seeing via miniature eye movements: a dynamic hypothesis for vision. Front Comput Neurosci 6: 1–27.

16. Rucci M, Victor JD (2015) The unsteady eye: an information-processing stage, not a bug. Trends Neurosci 38: 195–206.

17. Greene E (2018) New encoding concepts for shape recognition are needed. AIMS Neurosci 5: 162–178.

ISSN - 2373-7972

Cognitive conflict and restructuring: The neural basis of two core components of insight

Amory H. Danek1,* and Virginia L. Flanagin2
1 Experimental and Theoretical Psychology, Universität Heidelberg, Heidelberg, Germany
2 German Center for Vertigo and Dizziness (DSGZ), Klinikum der Universität München, Marchioninistr. 15, 81377 Munich, Germany

A B S T R A C T

Sometimes, the solution to a difficult problem simply pops into mind. Such a moment of sudden comprehension is known as "insight". This fundamental cognitive process is crucial for problem solving, creativity and innovation, yet its true nature remains elusive, despite one century of psychological research. Typically, insight is investigated by using spatial puzzles or verbal riddles. Broadening the traditional approach, we propose to tackle this question by presenting magic tricks to participants and asking them to find out the secret method used by the magician. Combining this approach with cueing in an fMRI experiment, we were able to break down the insight process into two underlying components: cognitive conflict and restructuring. During cognitive conflict, problem solvers identify incongruent information that does not match their current mental representation. In a second step this information is restructured, thereby allowing them to correctly determine how the magic trick was done. We manipulated the occurrence of cognitive conflict by presenting two types of cues that lead participants to either maintain their perceptual belief (congruent cue) or to change their perceptual belief (incongruent cue) for the mechanism behind the magic trick. We found that partially overlapping but distinct networks of brain activity were recruited for cognitive conflict and restructuring. Posterior, predominantly visual brain activity during cognitive conflict reflected processes related to prediction error, attention to the relevant cue-specific sensory domain, and the default brain state. Restructuring on the other hand, showed a highly distributed pattern of brain activity in regions of the default mode, executive control networks, and salience networks. The angular gyrus and middle temporal gyrus were active in both cognitive conflict and restructuring, suggesting that these regions are important throughout the insight problem solving process. We believe this type of approach towards understanding insight will give lead to a better understanding of this complex process and the specific role that different brain regions play in creative thought.

Keywords: insight; problem solving; restructuring; cognitive conflict; fMRI

1. Introduction

Moments of sudden enlightenment are known as "insight" or "Aha! moments". Typically, after struggling with a difficult problem for a long time, the solution pops into mind suddenly and effortlessly, offering a completely new perspective on the seemingly unsolvable problem. Creative insight is an

essential facet of human thinking and can be regarded as a ubiquitous process which is highly relevant for the scientific, technological or cultural advancement of society. Unfortunately, a feature of insight is that it occurs rarely, making it a difficult process to study systematically. Insight can be defined as a "complex, non-linear transition process that consists of an affective component (the subjective Aha! experience) and a cognitive component (the sudden representational change or restructuring leading to a correct solution)" [1]. While it has been shown that the subjective Aha! experience is not always present during the solution process [2], the cognitive component (i.e. restructuring the mental problem representation from an initially incorrect one to a correct one) can be considered essential for solving the problem. Thus, we focused on the cognitive component of insight, without assessing the affective Aha! experience. An additional reason for this decision was that cues have been shown to alter solvers' subjective experience of the solution process [3,4], letting Aha! ratings appear as a less useful measure in the present study which used cues as main manipulation. The aim of the present study was to break down the cognitive component of insight into two underlying cognitive processes thought to be crucially involved in insight problem solving and to look for neural activity specific to each of them: Cognitive conflict and restructuring.

"Cognitive conflict" in insight problem solving must be differentiated from response conflict where a decision has to be made between several competing actions, as for example in the Stroop task [5]. Rather, while working on a problem, solvers may detect incongruent information which does not fit with the current mental representation of the problem. This realization is likely to produce cognitive conflict. In some cases, this conflict cannot be resolved, leading problem solvers into an impasse. To resolve this conflict, the initial view on the problem must be modified which opens up new solution possibilities. Thus, detecting and processing cognitive conflict is likely to be one of the key processes involved in insight. In other words, cognitive conflict is needed in order to trigger a change in the problem representation, as postulated by Luo and Knoblich [6].

Conflict detection is a prerequisite of restructuring, which can be defined as "a change in the problem solver's mental representation of the problem" [7] or simply as "structuring again" [8]. The Gestalt psychologists were the first who described this cognitive process as a fundamental change in thinking which drastically alters the solver's view on a given problem—"Umzentrieren", i.e. "recentering", as Max Wertheimer put it [9]. There is wide-spread agreement that restructuring is crucial for insight, for example Luo and Knoblich stated that "The process of restructuring is regarded as the essential feature of insight problem solving" [6]. Restructuring is the key process in the representational change theory of insight [7,10–12] which has given the Gestalt tradition a modern, more precise and testable form. Ohlsson [11] has suggested different mechanisms how a problem representation can be restructured, for

example by relaxing unnecessary constraints, directing attention towards the relevant problem features, recombining information or perceptual re-groupings of problem elements. Restructuring implies that the initial way of thinking about a problem must be overcome (since it does not lead to the correct solution) and be changed by new combinations of the given information. If a problem that initially triggers an incorrect representation is eventually solved correctly, we can infer that restructuring has taken place. Only few studies exist so far that have tried to identify neural correlates of restructuring. An EEG study by Sandkühler and Bhattacharya [13] used self-reported restructuring and found right prefrontal activity. However, it is doubtful whether participants are able to consciously report on their experience of restructuring which is thought to mainly rely on unconscious processing [12].

Indeed, there is evidence that insight problem solving proceeds in an all-or-none fashion, with no partial solution information being available to the solver before the full solution is reached [14]. In the same vein, Metcalfe [15] found that solvers were not even able to predict their eventual success on insight problems nor were they able to correctly report their progress via feeling-of-warmth ratings [16]. It is for that reason that we chose, in the present study, not to operationalize restructuring through self-reports, but to rely instead on the more objective measure of solution rates, or to compare correct with incorrect solutions: solved with unsolved trials. By using a task which inherently triggers an initially incorrect problem representation that can only be solved if restructured, the occurrence of restructuring is inferred from whether the problem was correctly solved or not. If the problem is not solved (or not solved correctly), no restructuring has taken place. If the problem is solved correctly, restructuring has taken place. This design is similar to the Sandkühler study where she used a comparable contrast that she called "Deeper understanding" [13] as well as to another recent study by Tik et al. [17].

In addition to restructuring, this study also examined cognitive conflict using the common approach of giving cues to manipulate participants' mental representations [4]. Conflict was manipulated by presenting either incongruent cues that provide conflicting information, or congruent cues that produce no conflict (compare Methods). Congruent cues were consistent with participants' initial, faulty problem representation whereas incongruent cues contained new information that contradicted the initial way of thinking about the problem. Only the incongruent cues produce a cognitive conflict by forcing participants to question their initial problem representation. This conflict can be resolved by initiating a restructuring which may then enable solvers to find a solution.

The studies that have so far investigated the neural basis of insight have led to highly diverse results. The first studies focused on verbal tasks and already multiple brain regions were found, among them the right anterior superior temporal gyrus (STG) [18], left supramarginal gyrus and the anterior cingulate cortex,

ACC [19], superior occipital gyrus, temporal gyrus, angular gyrus, precuneus, many frontal areas and the ACC [20] and the left lateral PFC as well as the ACC [21]. Reviewing the existing fMRI data, Dietrich and Kanso [22] concluded that while the ACC was consistently found and the STG was reliably activated at least by one type of verbal problems, these findings remained very heterogeneous and no clear picture emerged with regard to a more general basis of insight. Additionally, a right-hemispheric dominance had been postulated for insight [23,18,24], Dietrich and Kanso [22] however concluded that there is no support for this claim, neither in the reviewed electrophysiological data nor in the neuroimaging data.

Because all of the aforementioned studies implemented tasks from only one domain (verbal), these findings might be partially task-specific. A more recent quantitative meta-analysis on insight by Sprugnoli et al. [25] compared results across different task domains. They came to a similar conclusion as Dietrich and Kanso [22], that there was no evidence for right-brain dominance, and that the brain regions recruited for insight were highly diverse. According to this review, the following regions were all involved in insight problem solving: Precentral gyrus, middle temporal gyrus, precuneus, cingulate gyrus, claustrum, middle occipital gyrus, uvula (inferior vermis—cerebellum) and insula (all left hemisphere) and superior frontal gyrus, insula, precuneus and middle temporal gyrus (right hemisphere).

One reason for the lack of convergence across studies may be the widely differing designs and contrasts used. For example, in the Sprugnoli meta-analysis, the operationalization of "insight" ranged from giving cues [21] or showing solutions [26] to choosing between different solution alternatives [27] or comparing self-reported "Aha! solutions" with "no Aha! solutions" [28,18]. Obviously, it is highly questionable whether these studies assessed insight in a comparable manner and thus the inconsistency is not very surprising. A perhaps more promising approach could be to tackle the individual components of this complex thinking process separately before trying to understand the bigger picture of insight.

The present study was designed with the aim of locating neural correlates of two individual components, cognitive conflict and restructuring, of the insight network. We tested whether neural activity would vary as a function of cue type to examine cognitive conflict. In addition, we aimed at identifying brain areas active during restructuring. Given the fact that there is no clear evidence for hemispheric dominance in insight problem solving [22,25], we did not set up any specific hypotheses regarding laterality.

The present study implemented a set of magic tricks as a problem-solving task, asking participants to find out the secret method used by the magician. We have previously shown that magic tricks are well suited to investigate insight problem solving [1,29] and have used them previously in a passive viewing paradigm to examine the neural correlates of expectation violation [30]. To gain insight into a magic trick requires a representational change, typically a change of conceptual knowledge about objects, e.g. realizing that a seemingly solid ball is only a half ball. The initial mental representation of the problem which is typically incorrect must be restructured into the correct problem representation which then allows to solve the problem. Following this rationale, we argue that magic tricks represent ideal material to investigate insight and specifically, the restructuring process, as also outlined by Danek [1]. In order to be able to trigger cognitive conflict and, subsequently, restructuring, a cueing paradigm was used, as described above. Behaviorally, we expected higher solving rates after incongruent cues, as compared to congruent ones. With regard to neural activity, we expected that the incongruent, but not the congruent cue will lead to cognitive conflict. Thus, neural correlates of cognitive conflict in insight problem solving will be identified through the following contrast: Incongruent cue (cognitive conflict) > congruent cue (no cognitive conflict). Neural correlates of restructuring in insight problem solving will be identified through the following contrast: Correct solutions (restructuring) > incorrect solutions (no restructuring).

2. Materials and method

2.1. Participants

Thirty-two healthy right-handed adults (mean age: 23.2 yrs, range 19–30 yrs; 16 male) participated in this experiment. Participants were only recruited if they had no contraindication for entering the MRI room (non-removable metal) and no history of neurological disease. All participants gave written informed consent to participate in the study, according to the Declaration of Helsinki, and were monetarily compensated with 20.-Euro for their time. The study was approved by the ethics committee of the medical faculty of the Ludwig-Maximilians-Universität München (#109-10). Two participants were excluded from the analysis because they stated in the solution phase (see Figure 3 and Procedure) that they had known the solution already before the cue was shown for 17 and 16 out of 20 tricks, respectively. In these participants, the number of trials in which cognitive conflict and restructuring could have occurred were too low for the analysis. The remaining 30 participants (mean age: 23.3 yrs, range 19–30 yrs; 15 male) were used in the analysis.

2.2. Testing material

2.2.1. Magic tricks

A set of 20 magic tricks was presented to participants as a problem-solving task (“Please try to find out how the trick works!”). The material consisted of short video clips of magic tricks that were performed by a professional magician and recorded in a standardized setting. Clips ranged from 6.3 to 42.5 s. The magic stimuli covered a wide range of different magic effects (e.g. transposition, levitation, vanish) and techniques (e.g. misdirection, gimmicks, optical illusions). This paradigm has been established as a relatively new domain for insight problem solving [31]. All magic tricks used are difficult problems with low solving rates, with the characteristic that the initial, seemingly obvious problem representation does not lead to a correct solution.

In the following description of the experiment, we will give an example of one magic trick from our stimulus set (the “Ball Trick”). In this trick, the magician shows a little red ball to the audience (see Figure 1). Apart from the ball, his hand is empty. He then holds the ball up in the air, shakes his hand and produces a second ball. The ball has seemingly multiplied. How can this be? Typical viewers of this trick perceive the balls incorrectly, assuming that both are round, solid objects. Amodal volume completion [32,33] is thought to be the perceptual mechanism behind the “Ball Trick”. Although only the front side of the ball can be seen, prior knowledge suggests that it looks identical from all sides. This constitutes a false mental problem representation. In reality, only half a ball exists, or rather just the shell of a ball, empty, with the second, slightly smaller ball stuck inside. During the shake, the two balls get separated and the second ball “appears” next to the first.

To correctly understand or “solve” a magic trick, insight and restructuring must take place: the mental representation of the solid ball must be discarded and substituted with the concept of half a ball covering another one. Many magic tricks exploit the fact that it is very hard to overcome these automatic assumptions [34].

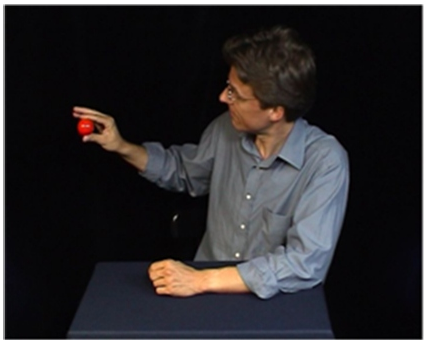

Figure 1. Example trick from the stimulus set. Screenshots from the initial (left) and the final (right) phase of the trick. In the video clip, the magician lets the little red ball multiply by simply shaking his hand. (see also http://www.youtube.com/watch?v=3B6ZxNROuNw for another example video clip)

2.2.2. Cues

We have shown previously that solution rates, or the number of times an individual can correctly restructure their knowledge, can be increased by providing verbal hints after the viewing of the magic trick [29]. In a follow-up study, we found that pictorial cues were even more helpful than verbal cues [35]. In the present study, we therefore used only pictorial cues. In two pilot studies, we developed and refined the cues. In these pilot studies, magic tricks were presented one time and visual cues were given that either confirmed the perceptual mechanism behind the magic trick (congruent cue), or that could help them to find the real solution to the magic trick (incongruent cue—see below). Helpful, incongruent cues roughly doubled the solution rates as compared to unhelpful, congruent cues. In the present study, two different types of cues were implemented:

a) Congruent cue: This cue is congruent with the typical problem representation and does not offer any contradicting information. Basically, the principle of the magic effect that was just witnessed is repeated. For example, in the ball trick, the congruent cue (see Figure 2 left) illustrates the effect of "multiplying" by showing a number of little bunnies as the offspring of one bunny. Through this cue, participants are encouraged to stick with the initial problem representation of "several different solid balls" that prevents a correct solution. The cue does not trigger a cognitive conflict and is therefore not helpful.

b) Incongruent cue: This cue offers new information that contradicts participants' initial problem representation and thus leads to cognitive conflict—a prerequisite for restructuring the problem representation and gaining insight into the correct solution. It is therefore a helpful cue. For the ball trick, this is a picture of several Matryoshka dolls, inducing the idea of sticking objects into one another (Figure 2 right).

Only the incongruent cues will force participants to re-consider their perception of the problem, restructure it and thus enable them to gain insight into the trick.

Figure 2. The two different cues used for the ball trick from Figure 1. Left: The congruent cue. The rabbits are multiplying like the red balls. Right: The incongruent cue. Matryoshka dolls are built so that the next size fits into the previous one, suggesting that multiple objects can be contained within one.

2.2.3. Trick selection

The set of 20 magic tricks (and their corresponding cues) for this study were selected from a larger set of 34 magic tricks based on the two pilot studies mentioned above. To be selected, the solving rate after the incongruent, helpful cue had to be 25%. Further, using the unrelated dataset from another study by Danek and Wiley [36] where participants (n = 70) had the possibility to see each trick up to three times before attempting to solve, we checked the spontaneous solution rates of the selected tricks after one single viewing. For the 20 selected tricks, these were all below 13% (with a mean of 2.9%).

2.3. Experimental design

The study was set up as a within-subjects design, so that each participant would be presented with 20 magic tricks (10 with an incongruent, helpful cue, 10 with a congruent, unhelpful cue). However, due to a numerical error in the seed randomization file, the actual ratio was 9:11 for each participant. Since conditions were switched after each participant, so that for the next participant, each trick would be shown in the alternate condition, this next participant had the ratio reversed (11:9). The next person had 9:11 again and so on. Therefore, across all participants, each trick was still presented in 50% of the cases with an incongruent cue, and in 50% with a congruent one. Trick order was randomized for each participant to control for learning effects.

Our data analysis was not impacted by this error, because each participant could solve an arbitrary number of tricks (individual solution rates ranged from 3 to 12 tricks). Therefore, the number of correct/incorrect solutions included in the analyses varied between participants. Further, we used mixed models, so that analyses were done on the level of observations and participants were modelled as a random effect. Overall, after excluding some more individual trials due to noise etc., the final

distribution of trials across the two conditions was nearly equal (572 valid observations, 285 in the incongruent condition, 287 in the congruent condition, as stated in section 2.9.).

2.4. Procedure

Each trial consisted of three phases, exposure, cue and solution phase, always in that order, in a block design (Figure 3). In the exposure phase, participants were presented with the problem once (one viewing of the magic trick clip), to set up a mental representation of the problem. This phase was between 6 and 42 seconds, depending on the clip. After a 1 second fixation, the 16 second cue phase followed, where the cue picture was presented. Finally, the solution phase immediately followed the cue phase, where participants verbally provided a solution and also answered two more questions within 30 seconds. All tasks were difficult problems with low solving rates, with the feature that the first, seemingly obvious problem representation does not lead to a correct solution. Thus, the problems used are typically not solvable after the first viewing.

In the scanner, participants were presented with 20 video clips of magic tricks, after an instruction to watch the clip carefully in order to find out how the trick works. They were also told that after each magic trick, a picture would be visible that could be either helpful for solving the magic trick or not. Either a helpful or unhelpful cue was then presented. Figure 3 shows the sequence of one trial. After each cue phase, the solution phase began. A solution screen appeared with the following three questions (translated from German): "1. Was the picture helpful? 2. Did you know the solution already before you saw the picture? 3. If you have a solution, please describe it now!" Participants were instructed to answer the questions verbally by speaking into a microphone. With insight problems, free verbalisation is the only way for participants to provide behavioral feedback that can be used for further analysis, which is why we chose this method. We separated the cue and the solution phases in order to temporally segregate the verbalisations and motor planning from the problem solving itself and to reduce motion confounds in the phase of the trial we were interested in. Together with the preparation phase (safety instructions for participant and practice trials) and the anatomical scan, each scanning session lasted about two hours.

2.5. Coding of solution accuracy

Using a coding manual (compiled with the help of the magician), participants' solutions were coded as correct (methods that the magician actually used or alternative methods verified as plausible) or incorrect (partial solutions, implausible methods, or impossible solutions with respect to the conditions seen in the video clip) by two independent raters. The two-way random intraclass correlation coefficient

(absolute agreement), ICC (2, 2) was 0.97 with a 95% confidence interval of [0.97;0.98] indicating an excellent level of agreement according to the conventions set out in Koo and Li [37]. Conflicting cases were resolved by a third rater.

2.6. Experimental setup

The experiment, timing and synchronisation was programmed in python, presented on a Dell Latitude E6530 (64 bit) laptop computer running Windows 7. Magic clips and cues were presented to participants in the MRI machine via a back-projection system from a projector (Christie LX40) with True XGA 1024 × 768 resolution. While the solution screen was visible, participants could verbally respond to the three questions given. Their responses were recorded by an MRI compatible optical microphone (Sennheiser MO 2000, Wedemark, Germany) and amplifier (Sennheiser MO243 2000 CU) directly onto the same laptop computer. Only the 30 seconds of the solution phase were recorded.

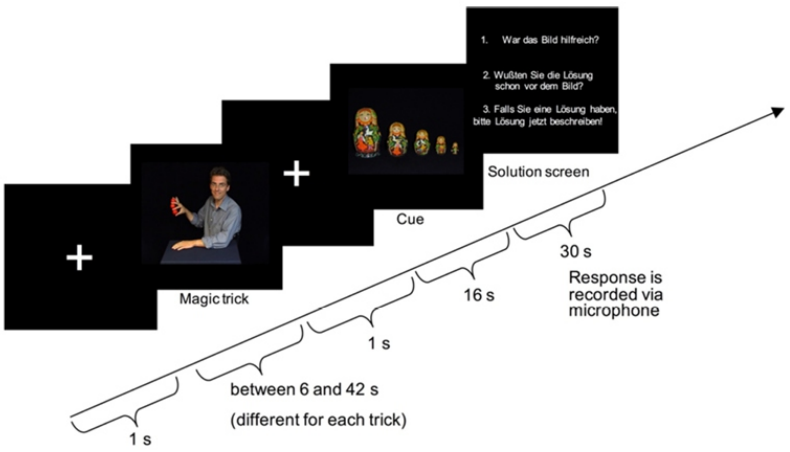

Figure 3. Sequence of one trial. Each trial started with a fixation cross followed by the magic trick of variable length (exposure phase). Then after an additional second of fixation, the cue phase started, where a cue was presented for 16 seconds, during which participants tried to solve the magic trick. Immediately after cue presentation, the solution phase began, where participants saw the three questions that they verbally responded to (see Procedure).

2.7. Imaging data acquisition

Functional imaging data were acquired on a 3T MRI Scanner (Signa HDx, GE Healthcare, Milwaukee, WI, USA) with a standard 8-channel head coil. A BOLD-sensitive gradient echo echoplanar-imaging sequence was used to collect 597 volumes thirty-seven contiguous transverse slices of functional data (TR 2.0 s, TE 40 ms, flip angle 80 deg. Matrix 64 × 64 voxel, FOV 200 mm, 3.125 × 3.125 mm within-

slice voxel size, 3.5 mm slice thickness, no gap). The first four functional images were not reconstructed to avoid T1 effects and are therefore not part of the final volume number. The experiment started synchronized to the fifth functional image. An additional 3D T1-weighted highresolution structural image with 0.8 × 0.8 × 0.8 mm isotropic voxel size, was collected after functional imaging for normalization and visualization purposes.

2.8. Imaging data analysis

Functional imaging data were analyzed using SPM12, (version 7219, Wellcome Department of Imaging Neuroscience, University College London) on Matlab 8.2.0.701 (R2018a). The SPM12 default settings of each preprocessing step are used, unless otherwise specified. To improve coregistration performance, all images were manually reoriented so that the origin was set to the anterior commissure prior to preprocessing. Then the functional volumes were slice time corrected, realigned to the first volume of the first run and then to the mean across all runs. They were then coregistered to the anatomical image from each subject. The anatomical image was segmented into tissue probability maps based on standard stereotaxic space [Montreal Neurological Institute (MNI)], creating tissue subject-specific probability maps for grey matter, white matter, cerebrospinal fluid (CSF) bone and soft tissue. The inverse deformation field created during segmentation was used to normalize the functional volumes. Images were resampled to 2 × 2 × 2 mm isotropic voxels during normalization. Noise was reduced by smoothing the functional data using an 8-mm full-width at half-maximum Gaussian kernel.

Functional data were analyzed in each single subject block design using univariate multiple regression. The three experimental phases, the magic trick exposure, the cue phase and the solution phase, were all modeled as blocks with length: variable, 16 s, and 30 s respectively. However, we focused on the cue phase of the experiment (Figure 3), dividing this phase of the trials into separate regressors depending on the experimental condition, because the cue phase was where we expected both cognitive conflict and restructuring to occur in this design. The study was conceived as a 2 × 2 (congruence x solved) factorial design, which was originally carried through in the data analysis. For this first analysis, four regressors were created corresponding to trials that were congruent solved, congruent unsolved, incongruent solved and incongruent unsolved. Individual subject regression models included these four regressors, as well as the regressors of no interest in the final regression models used below. When analyzing the subject reports however, we found a higher rate of solving the tricks prior to the cue than in the pilot studies. We wanted to remove the previously solved trials for the question of restructuring. However, with the 2 × 2 factorial design it would have resulted in regressors in many subjects with 0–2 trials. We therefore chose instead to analyze the data as two separate models, one to test for brain areas

corresponding to cognitive conflict, and one to test for regions that are recruited during restructuring.

In the first model, we modeled congruent and incongruent cue trials as separate regressors of interest to examine the brain regions recruited during cognitive conflict. All trials were categorized by the cue, independent of how they were solved. In the second model, we modeled the cue phase separately for three different types of trials. One regressor corresponded to trials in which the participant solved the magic trick correctly, a second for trials in which the participant did not solve the trick or solved it incorrectly, and one for trials in which the trick was solved before the cue phase. Both models additionally included movement parameters that modeled residual BOLD signal variability. Data were high-pass filtered (cutoff frequency = 0.0078 Hz) to minimize slow scanner related drifts. Global changes were removed by proportional scaling. For each subject, we computed subtractive contrasts of interest (Model 1: incongruent–congruent, Model 2: correctly solvedincorrectly solved) which were then entered into two group-level general linear models. T-tests for the difference between incongruent and congruent, and correct and incorrect were used to test for significant activity at the group level. Because of inter-subject differences in the solving rates, solving rate was additionally added as a regressor to the correct-incorrect group model.

The significance level was set to $p < 0.05$, FWE corrected at the cluster level. First, a voxel-level primary threshold of $p < 0.001$ was used to create clusters. Then under the null hypothesis of no signal, random field theory was used to estimate the largest null cluster size, given the smoothness of the data [38,39]. Only voxels within the brain mask and outside of a CSF-mask (created by thresholding the MNI-template CSF probability map at 0.5) were considered in the analysis.

Anatomical regions were identified using the Anatomy toolbox (Version 2.2b) [40] for SPM and cross-checked with activity patterns in Neurosynth (http://neurosynth.org/). For frontal and prefrontal regions that have alternative labeling schemes than in the Anatomy toolbox, such as the dorsolateral prefrontal cortex (DLPFC), we compared our results to the MarsAtlas [41], the Brannetome Atlas (http://atlas.brainnetome.org/index.html) and to the delineations in the literature [42,43].

2.9. Behavioral data analysis

For all analyses of behavioral data, mixed effects models were used. This approach has the advantage that it takes into account the hierarchical structure of the present data, in this case by modelling participants as random effects, fitting random intercepts for participants.

In total, 30 participants were presented with 20 tricks which yielded 600 observations. On the level of individual observations, seven observations could not be used for the analysis, because the low audio quality of the recording made it impossible to determine participants' responses. For the behavioral analysis, an additional 21 observations were excluded because participants indicated that they were already familiar with the solution to the trick, leaving 572 valid observations (285 in the incongruent condition, 287 in the congruent condition). Of those, 29.0% (166 observations) were not solved (i.e. no answer provided), 42.3% (242 observations) were correctly solved, and 28.7% (164) were incorrectly solved.

3. Results

3.1. Manipulation check

We first checked whether participants in the two cue conditions differed in their perception of the cue by using a mixed-effects model to perform a binary logistic regression on the question of how helpful the picture was (a categorical measure). We included cue condition as fixed effect and fitted random intercepts for subjects ($Z = 1.30$, $p = 0.20$). As intended, the helpful cue was perceived as more helpful ($M = 0.72$, $SD = 0.45$) than the unhelpful cue ($M = 0.26$, $SD = 0.44$), with $F(1, 570) = 107.33$, $p < 0.001$, Cohen's $d = 0.87$ (level of analysis is observations, number of observations = 572).

3.2. Behavioral results

An analogous analysis was run on the variable solution correctness. As expected, helpful, incongruent cues led to higher solution rates ($M = 0.59$, $SD = 0.49$) than the unhelpful, congruent cues ($M = 0.26$, $SD = 0.44$), with $F(1, 570) = 58.81$, $p < 0.001$, Cohen's $d = 0.64$ (number of observations = 572).

3.3. fMRI analyses

3.3.1. Cognitive conflict

We first examined the influence of cue on brain activity by comparing the activity during incongruent cues and congruent cues. We found no significant brain activity for congruent cues compared to incongruent cues. This is in line with the idea that the congruent cues do not provide any additional knowledge to the participant; they represent the most common perceptual model of the trick. Incongruent cues, on the other hand, provide a conflict to the perceptual model of the magic trick.

brain areas, bilaterally, extending into the thalamus, hippocampus and temporal lobes (Figure 4). In addition, bilateral frontal activity could be seen, including the frontal eye fields [44] and extending into the dorsolateral prefrontal cortex (DLPFC). A list of the clusters of activity can be found in Table 1. Most of the activity was found in early visual areas. This is surprising, given that, although the same cues were used for each magic trick, each participant had a different randomization of what magic tricks were paired with congruent or incongruent cues. This means that although each trick had only one congruent and one incongruent cue, different participants saw different parings. Therefore, the effects we see are not likely related to visual differences in the cues themselves.

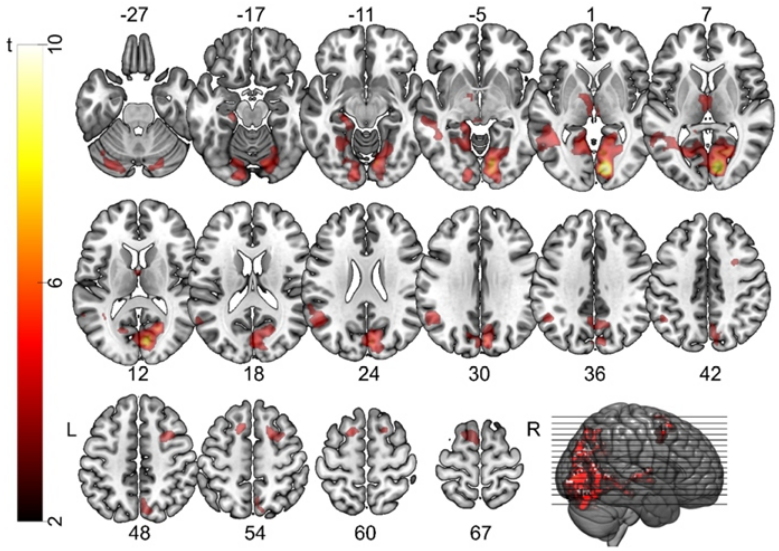

Figure 4. Activity patterns for cognitive conflict. Areas significantly more active during presentation of the incongruent cues compared to the congruent cues. Activity is thresholded at $p < 0.001$ voxel-wise and $p < 0.05$ FWE-corrected cluster-wise significance levels and overlaid onto a brain extracted version of the MNI152 template brain.

Table 1. Brain regions recruited during cognitive conflict. Peak voxels and corresponding brain regions that were significantly more active for incongruent vs. congruent cues. Magic tricks that were familiar to the participant were removed from the analysis. IPL: inferior parietal lobule, hOc1-3: human occipital cytoarchitectonic areas 1–3, corresponding to V1, V2 and V3 respectively, PGa, PFm & PFcm, cytoarchitectonically distinct areas of the inferior parietal lobe [45]. Coordinates are given in mm MNI space. Secondary peaks that do not have cluster sizes or p-values are sub-peaks within the current cluster.

Anatomical region	Cluster size	Coordinates (MNI) (mm)			Peak voxel		p-value (clus.)
	# voxels	x	y	z	T-value	z-score	p(FWE-corr)
R lingual gyrus, visual cortex, V1, BA17, Area hOc1 (V1)	7668	14		-82	4	9.86	6.48	0
R Area hOc2 (V2), Area hOc3 (V3)		10		-64	4	6.6	5.12	

R Area hOc1 (V1)		22	-66	10	6.59	5.11	
R lingual gyrus, anterior -towards medial temporal lobe		14	-54	4	6.19		
R lingual gyrus, anterior - towards medial temporal lobe		16	-52	2	6.09		
R precuneus		6	-82	26	6.03		
L Area hOc3v [V3v]	924	-12	-88	-6	5.27	4.38	0
L cerebellum, lobule VIIa, Crus I & hOc3 (V3)		-14	-90	-14	5.23	4.35	
L cerebellum, lobule VIIa, Crus I		-28	-80	-26	4.98	4.2	
L cerebellum, lobule VI		-16	-76	-16	4.86		
L cerebellum, crus I		-38	-66	-30	4.03		
L cerebellum, crus I		-40	-64	-24	3.91		
L middle temporal gyrus, Area PGa (IPL)	517	-48	-56	26	5.24	4.36	0.003
L angular gyrus, Area PF (IPL) into Area PFm (IPL)		-48	-54	38	4.76	4.06	
L superior temporal gyrus, and into Area PFcm (IPL)		-60	-42	24	3.7	3.32	
L superior frontal gyrus, Area 6, dorsolateral	294	-16	12	60	5.18	4.32	0.032
L superior frontal gyrus		-14	14	56	5.03		
L posterior-medial frontal gyrus, dorsomedial prefrontal cortex (dmPFC)		-6	6	68	4.02	3.55	
L superior frontal gyrus		-16	6	68	3.83	3.41	
R superior frontal gyrus	341	20	8	54	4.76	4.06	0.019
R superior frontal gyrus, Area 6		18	16	58	4.7	4.02	
R middle frontal gyrus, dorsolateral prefrontal cortex (DLPFC)		32	8	48	4.48	3.87	

3.3.2. Restructuring (correct vs. incorrect)

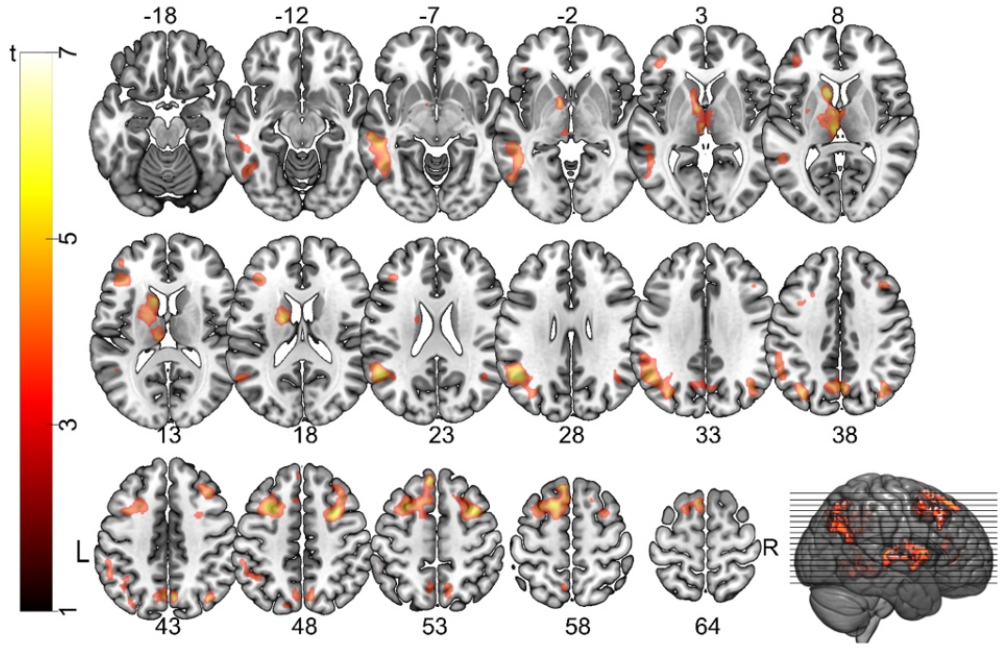

Figure 5. Activity patterns for restructuring. Areas significantly more active during the cue phase on correct trials compared to incorrect or not solved trials. Brain activity is more widespread and less posterior than in the previous contrast. Activity is thresholded at $p < 0.001$ voxel-wise and $p < 0.05$ FWE-corrected cluster-wise significance levels and overlaid onto a brain extracted version of the MNI152 template brain.

In a second analysis step, we compared the brain activity on trials where participants correctly solved the magic trick to trials where the magic trick was not correctly solved (either not solved or incorrectly). Trials in which participants reported to have solved the trick before the cue period started (see the solution phase in Figure 3) were modelled separately as trials of no interest, but not included in the comparison between correct and incorrect trials. No brain regions were significantly more active during incorrect trials compared to correct trials. In contrast, a widespread network of brain regions across the entire brain were recruited for correct trials compared to incorrect trials. Frontal, temporal and parietal cortical regions were significantly active, as well as the thalamus and the basal ganglia (Table 2, Figure 5).

The brain regions partially overlapped with regions that were significantly more active during incongruent cues. These regions include the frontal eye fields extending into the DLPFC and the medial temporal gyrus bilaterally. The early visual areas were no longer active for restructuring, but rather higher visual and parietal areas. Many more frontal regions were active during restructuring than during cognitive conflict.

Table 2. Brain regions active during restructuring. Peak voxels and corresponding brain regions that were significantly more active on correct trials than on incorrect trials. Trials that were solved before the cue was presented were not included in this contrast. IPS: inferior parietal sulcus, FG: frontal gyrus, MFG: medial frontal gyrus, SPL: superior parietal lobe, IFG: inferior frontal gyrus, MTG: medial temporal gyrus, ITG: inferior temporal gyrus. Coordinates are given in mm MNI space. Secondary peaks that do not have cluster sizes or p-values are sub-peaks within the current cluster.

Anatomical region	Cluster size	Coordinates (MNI) (mm)			Peak voxel		p-value (clus.)
	# voxels	x	y	z	T	Z-score	p(FWE-corr)
L caudate nucleus	1214	-10	14	10	6.86	5.21	0
L thalamus, temporal and prefrontal part		-2	-20	6	6.19	4.87	
L putamen		-12	2	-4	6.04	4.79	

L middle temporal gyrus, Area PGa (IPL)	1349	-48	-56	28	6.41	4.99	0
L middle temporal gyrus		-52	-56	24	6.34		
L middle occipital gyrus, possibly Area PGa (IPL)		-34	-72	36	5.04	4.22	
L inferior parietal lobule, Area hIP1 (IPS)		-38	-52	46	4.31	3.74	
L supramarginal gyrus, Area PF (IPL)		-56	-44	36	4.30		
L supramarginal gyrus, Area PFm (IPL)		-54	-52	40	4.22		
L superior medial gyrus, rostral medial prefrontal cortex (PFrm), Area 9m	1440	-6	36	54	6.39	4.98	0
L superior frontal gyrus, dorsomedial prefrontal cortex (dmPF), Area 8m		-14	14	58	5.81	4.67	
L middle frontal gyrus, dorsolateral prefrontal cortex (DLPFC)		-30	12	48	5.69	4.6	
L posterior frontal gyrus, dorsomedial prefrontal cortex (dmPFC)		-8	18	62	4.75		
L posterior medial gyrus, dorsomedial prefrontal cortex (dmPFC)		-12	6	56	4.71		
L posterior medial gyrus, dorsomedial prefrontal cortex (dmPFC)		-4	14	64	4.58		

Continued on next page

Anatomical region	Cluster size	Coordinates (MNI) (mm)			Peak voxel		p-value (clus.)
	# voxels	x	y	z	T	Z-score	p(FWE-corr)
R middle frontal gyrus, dorsolateral prefrontal cortex (DLPFC)	661	36	8	52	5.95	4.75	0
R middle frontal gyrus, dorsolateral prefrontal cortex (DLPFC)		30	6	48	5.8		
R middle frontal gyrus, dorsolateral prefrontal cortex (DLPFC)		38	26	42	4.6	3.94	
R middle frontal gyrus, dorsolateral prefrontal cortex (DLPFC)		36	20	48	4.43	3.82	
R middle frontal gyrus, dorsolateral prefrontal cortex (DLPFC)		32	30	46	4.39		
R superior frontal gyrus, dorsolateral prefrontal cortex (DLPFC)		18	20	54	4.21		
R precuneus	602	4	-70	42	5.67	4.59	0
R precuneus		10	-60	52	4.35	3.77	
L precuneus, possibly Area 7P (SPL)		-6	-62	54	4.12	3.61	
L superior parietal lobule		-14	-78	48	3.82		
Cerebellar vermis & lobule V	384	2	-68	2	5.33	4.39	0.006
L Middle temporal gyrus	859	-52	-34	-8	5.23	4.33	0
L middle temporal gyrus		-60	-28	-6	5.23	4.33	
L inferior temporal gyrus, possibly Area FG4		-46	-48	-4	4.97	4.17	

L inferior temporal gyrus		-48	-54	-6	4.82		
L inferior temporal gyrus, FG4		-46	-56	-8	4.69		
L inferior temporal gyrus		-54	-66	0	4.57		
L anterior insular lobe	316	-30	20	4	4.94	4.15	0.013
L inferior frontal gyrus (pars Orbitalis)		-26	24	-4	4.76	4.04	
L inferior frontal gyrus (pars Orbitalis)		-32	22	-8	4.25		
L temporal pole		-52	16	-6	4.21	3.67	
R angular gyrus, Area PGp (IPL)	266	38	-72	42	4.86	4.1	0.026
R angular gyrus, parts of Area PGp (IPL)		42	-68	36	4.58	3.93	
R middle temporal gyrus		42	-56	26	3.72	3.32	

Continued on next page

Anatomical region	Cluster size	Coordinates (MNI) (mm)			Peak voxel		p-value (clus.)
	# voxels	x	y	z	T	Z-score	p(FWE-corr)
L inferior frontal gyrus (pars Triangularis), ventrolateral prefrontal cortex (VLPFC)	356	-38	32	20	4.45	3.84	0.008
L inferior frontal gyrus (pars Triangularis), ventrolateral prefrontal cortex (VLPFC)		-40	30	14	4.38		
L middle frontal gyrus, ventrolateral prefrontal cortex (VLPFV)		-42	48	12	4.31	3.74	

4. Discussion

In this study, we systematically examined individual components of insight problem solving by introducing two types of cues that "prime" the participants to either maintain their perceptual belief (congruent cue) or to change their perceptual belief (incongruent cue) for the mechanism behind various magic tricks. In two pilot studies, these cues were developed and refined and magic tricks were chosen for their low spontaneous solution rates without cues and their intermediate solving rates with incongruent cues. Then in a separate experiment we tested naïve participants on these tricks and cues and measured their brain activity with fMRI. Behaviorally, across all participants, just under half of all of the trials were correctly solved. The incongruent cues were reported to be more helpful and had higher solution rates than the congruent cues. This finding supports the hypothesis that a cue which provides information which is incongruent with the solvers' initial mental representation of the problem triggers cognitive conflict and a subsequent restructuring of the problem representation which then often leads to a correct solution. Similarly, we found no significant brain activity for congruent or incorrect trials, compared to incongruent or correct trials, respectively. We did however find a predominantly visual network of activity for cognitive conflict (as reflected by an increased activity for incongruent trials), reflecting an increase in attentional control in the conflict situation on a perceptual level. Finally, a

widespread frontal, parietal and subcortical network was active during restructuring, as reflected by an increased activity for correctly solved magic tricks. Behaviorally speaking we can confirm and build on previous work that magic tricks provide a structured method for examining insight [1,29]. Magic tricks have been refined over centuries to reliably produce a state of incomprehension (and awe) after the first observation of a trick. Magicians skillfully lead observers towards an incorrect mental representation of what is happening which does not allow them to see through the magic trick. Here we can say that with the incongruent cues, an almost 50% solving rate could be achieved, which makes comparisons between correct and incorrect solutions, also for neuroimaging or electrophysiological experiments, more feasible than many other insight problem solving tasks. The increase in solving rates was due to the introduction of an incongruent cue that induced a cognitive conflict - a prerequisite for restructuring and, in this paradigm, for correct solutions. Our behavioral results are therefore in support of our neuroimaging design. The congruent cues which were specifically designed to be unhelpful worked as intended and led to rather low solving rates. This can be discussed in the light of other recent findings from the magic trick domain: Thomas et al. [46,47] demonstrated that exposure to a false solution prevented participants from discovering the true solution to a magic trick. This effect persisted even after they had been informed about the incorrectness of that false solution. It is possible that the congruent cues may have acted in a similar manner: Although they are not false solutions, the congruent cues strengthen the initial, inappropriate view of the magic trick and make it more difficult for problem solvers to break away from this view.

4.1. Neural correlates of cognitive conflict

We defined cognitive conflict as the brain activity during incongruent cue types compared to congruent cue types, as the congruent information contradicts participants' initial problem representation. We found a predominantly posterior visual network of brain regions, including the left hippocampus, regions of the temporal cortex, the thalamus and the frontal eye-fields bilaterally together with the DLPFC (Figure 4). These areas together suggest that the cognitive conflict aspect of insight problem solving primarily involves perceptual conflict. These regions have been found in activities such as visually guided behavior [48], control of spatial attention [49], perspective taking [50] and many other aspects of visual cognition [51]—although see the Limitations section for possible confounds with our design. Interestingly, the early visual areas were more active during incongruent cues, although the cues themselves were not different in their visual properties, and even differed between participants, depending on what magic trick was associated with a congruent or incongruent cue.

If we consider the brain regions that were active for cognitive conflict in a network setting, two predominant networks are active, the visual network, together with self-referential components of the default mode network including the temporal cortical areas and the angular gyrus [52]. Large portions of the default mode network have been shown to be active comparing solvable to unsolvable problems in the Compound Remote Associates Task in a recent study by Kizilirmak et al. [53] which can be compared to our cognitive conflict contrast. Contrary to Kizilirmak et al., the solution is not presented at this point, and therefore mind-wandering as in resting-state fMRI is not likely to be the cause of the DMN activity. There are two possible explanations for the activity in the default mode network during insight problem solving. Insight events benefit from removing constraints [10], or cessation of attempts to solve the problem, in which the mind must relax allowing for spontaneous restructuring and potential solution events. Alternatively, the DMN activation pattern we find may support associative memory. The posterior part of the DMN has also been termed the parietal memory network (PMN) [54] for its role in memory processes.

This explanation for the DMN activity complements the visual activation pattern found. In our cognitive conflict condition, the conflict arises from the initial problem representation and the incongruent cue. The participants would need to remember the magic trick that was given and associate that trick with the new information from the incongruent cue. This produces a perceptual conflict [55], in the Bayesian sense that prior sensory information, or visual memory, is in conflict with the current sensory information and the visual system attempts to resolve this conflict and reinterpret the sensory information that is received. Early as well as higher visual areas are thought to be involved in both associative visual memory and perceptual conflict resolution [56].

There are a number of important differences between cognitive conflict as it has been used in the literature, and the cognitive conflict that arises from the incongruent cues in magic insight problems. For instance, the flanker task is a classical example of cognitive conflict, where distractor words with the opposite semantic meaning flank the target word [57]. This conflict involves active control of cognition towards the target word and away from the incongruent flanker words, actively suppressing them, whereas our cognitive conflict contrast involves relinquishing control, allowing for new associations to be made. We believe this explains why we do not see more frontal activity in this contrast (although the DLPFC, a typical cognitive control region, was active), in particular in the anterior cingulate cortex (ACC) and the ventrolateral prefrontal cortex (VLPFC) as was found previously [57]. If the ACC is responsible for conflict monitoring and decision making [58], these processes do not necessarily occur in our cognitive conflict contrast.

In a meta-analysis on insight, Sprugnoli et al. found activity in temporo-occipital regions, in the middle temporal gyrus and in the frontal eye fields [25] that is specific to insight. The left angular gyrus (AG) has been found in insight problem solving in a comparable way. Kizilirmak et al. [59] contrasted correct solution words with pseudo-solution words, independent of participants' responses, similar to our cognitive conflict contrast. Another study [60] contrasted solved technical problems with a related "heuristic prototype" with unsolved technical problems with an unrelated "heuristic prototype". Both of these studies reported left angular gyrus activity.

A review by Seghier [61], based on meta-analyses and focusing on angular gyrus activity in healthy populations, describes the AG as a major connecting hub which is activated by a large number of different tasks. A key function which most consistently activates the left AG is semantic processing [62], also for visual stimuli [63]. In particular, the left AG is thought to be involved in concept retrieval and conceptual integration [62] which fits with the present task where a helpful concept (illustrated by the helpful, incongruent cue) needed to be retrieved and understood and then integrated into the mental representation of the magic trick. More interestingly, the AG was consistently found for conflict resolution [61]. In contrast to the right AG, the left AG is not activated by all conflicts (such as the classical go/no-go paradigm), but only by conflicts in a semantic context. Ye and Zhou [64] reported that left AG activity was triggered only by a conflict between plausible and implausible sentential representations.

The following possible function of the AG in processing incongruent vs. congruent cues in problem solving emerges: Multisensory input, in this case the perception of the pictorial cues, from lower brain levels such as the visual cortex, is integrated in the AG. Top-down predictions, based on prior knowledge, shape the integration. In the case of incongruent cues, the prediction (i.e. the mental problem representation) is at odds with the new information provided by the cue, causing cognitive conflict and a prediction error [65]. This does not happen for congruent cues since these simply reiterate the principle of the magic trick, which is in agreement with the viewer's existing problem representation and thus does not cause any conflict. This explains why left AG is activated only by the incongruent cues as compared to the congruent ones. It is important to note here as well, that we found no significant activity for congruent cues compared to incongruent cues, which is also in line with this theory.

4.2. Neural correlates of restructuring

To examine restructuring, we compared trials in which participants were able to arrive at the correct solution to trials in which they were not. Here, the activity was more widespread than for cognitive

conflict, in areas including the basal ganglia, the insula, parietal and temporal regions as well as more frontal regions. In general, the regions found in the two analyses did not show a large amount of overlap which indicates that we were actually tackling two different components of the insight process with the chosen contrasts.

Restructuring is closer to the actual "Aha!" or insight moment than is cognitive conflict. Therefore, more of the regions found for restructuring were also found in the meta-analysis of insight by Sprugnoli [25]. The middle and inferior frontal gyri (IFG, MFG) were found and suggested to be associated with memory, inhibition and task switching [66]. The anterior insula was also active during restructuring, a region known for its involvement in interoception and self-awareness [67].

The left medial frontal gyrus as well as the left middle temporal gyrus have also been found in a previous study [68], based on a comparable, but not identical, contrast. Tian et al. [68] compared the successful guessing of Chinese logogriphs to unsuccessful guessing. In contrast to the present study, participants did not actually provide the solution, instead, after trying to solve, the correct answer was presented and participants indicated whether they had thought of this answer or not. The authors interpreted this activity as related to breaking mental set or restructuring. Moreover, the medial frontal gyrus has been shown to be involved in creativity in another meta-analysis [69].

The left middle temporal gyrus (MTG) which represented one of the largest clusters for the restructuring contrast had previously been found by a recent study by Tik et al. [17] using the same contrast (i.e. solved vs. unsolved trials). Further, the MTG was one of the largest clusters of the insight network as outlined by Sprugnoli et al. [25]. The MTG also belongs to the salience network which supports dynamic switching between the default mode network and the executive control network [70]. Further, Beaty et al. [71] have implicated the MTG in creative cognition which fits with the idea of achieving a completely new view on a problem (restructuring it).

The activity found during restructuring partially overlapped with the regions found for cognitive conflict. This makes sense since we always considered the entire cue phase and did not look at restructuring only during or after it took place. The angular gyrus, middle temporal gyrus and frontal eye fields were present in both activity patterns, suggesting that activity in these regions are maintained throughout cognitive conflict and restructuring. All three regions were present in the meta-analysis of insight [25]. The dorsomedial thalamus was also active during cognitive conflict and restructuring but was not present in the meta-analysis. However, it is a region that is embedded in the salience network [72] and may therefore be relevant for both cognitive processes.

A number of regions also changed their statistical significance between the two cognitive processes. The early visual areas no longer reach significance for the correct trials, suggesting that visual attention, prediction error and comparing sensory input is no longer as relevant for restructuring as it was during cognitive conflict. Instead, frontal and parietal regions, together with the basal ganglia survived thresholding during restructuring. If we consider these regions from a network perspective, then the salience, executive function, and default mode network are all represented more during restructuring than during cognitive conflict. The medial prefrontal cortex and the precuneus are two highly connected hubs of the executive and default mode networks, respectively. Previous work shows that, although these two networks are anti-correlated at rest, a higher coupling between these two networks, and also with the anterior insula of the salience network supports the production of creative ideas [71]. It was suggested that the salience network helps to reallocate resources and allow for dynamic switching between the default mode network and the executive control network to promote creativity and insight [71,25]. We can add that this happens already at the phase of restructuring but likely not during cognitive conflict.

Two previous studies have examined brain activity during magic tricks [30,73]. Because both studies examined brain activity during passive viewing of magic instead of during the search for a solution, it is difficult to compare these studies to the current one. However, two regions of the brain are worth mentioning. First, both studies found the anterior cingulate cortex (ACC), a region that is often thought to be crucial for insight problem solving and many other cognitive tasks [67,25]. This region was speculated to be specifically active for conflict detection [30,73] which is likely why we do not find this region in our study, as the conflict detection had already occurred (since the cue directly pointed out the conflict). The basal ganglia, in particular the caudate nucleus, were also active during passive viewing of magic tricks and during restructuring. The caudate nucleus is thought to process changes in the contingency between an action and its outcome, primarily in order to perform successful goal-directed action [30,74]. This fits with our current results as well, where we would suggest a change in contingency during restructuring but not during cognitive conflict.

4.3. Limitations

Although we designed this study to the best of our ability to address the questions of interest, there are a number of limitations we would like to mention. Most importantly, we chose not to try and determine the actual "Aha moment" or the moment in which the participants solved the magic trick. This was primarily to avoid the motor confound in the imaging data that we would have had, if we had allowed subjects to give a response at any time. It is likely that additional brain regions, including the ACC, may be active

only for the time point of insight. For instance, the ACC was active for the individual time point of conflict detection in magic tricks [30,73]. Only with this additional time point can we really understand the brain state at the moment of insight.

Based upon the present results, we believe that using eye-tracking to monitor gaze behavior during cue viewing would provide additional important information about the different components of insight problem solving. The frontal eye fields were active for cognitive conflict and restructuring, suggesting a difference in gaze behavior between congruent and incongruent trials as well as between correct and incorrect trials. Additionally, pupillometry has been shown to relate to reward anticipation and correlate with activity in the salience network [75]. In future studies, recording pupil dilations may provide a time point of insight without a conscious motor response from participants.

5. Conclusion

In contrast to most neuroscientific studies investigating insight problem solving in its entirety, or in the single moment of the "Aha!" experience, the present study breaks down this complex process into two theoretically derived components to identify the neural correlates for each of them. Through this new approach, we succeeded in separating out the neural substrates for cognitive conflict from those for restructuring. This is not only a theoretically valuable result, but it may also help to resolve some of the inconsistency found across studies, as reflected in two current meta-analyses [22,25]. We found that brain activity during cognitive conflict reflected processes related to prediction error, attention to the relevant cue-specific sensory domain, and the default brain state. Restructuring on the other hand, was related to an interplay between the default mode and the executive control networks, that may be modulated by the salience network. The angular gyrus, middle temporal gyrus, frontal eye fields and DLPFC were all active in both cognitive conflict and restructuring, suggesting a more overarching role of these regions in the whole insight process. These results demonstrate the benefit of breaking down insight problem solving into its constituent processes to understand how the brain orchestrates such a complex cognitive task.

Acknowledgments

We thank Franziska Konitzer for writing the code for this experiment and Anna Gatz and Benedict Wild for their help with data collection and coding, for creating the pictorial cues as well as for conducting the pilot studies. We are indebted to magician Thomas Fraps (http://www.thomasfraps.com) for providing the magic trick stimuli. We thank Prof. Benedikt Grothe for valuable and insightful discussions. This

research project was funded by one grant to AD and another one to VLF from LMU Munich's Institutional Strategy LMUexcellent within the framework of the German Excellence Initiative. VLF is funded through the German Federal Ministry of Education and Research under the Grant Code 01EO1401.

Conflict of interest

The authors declare no conflict of interest.

References

1. Danek AH (2018) Magic tricks, sudden restructuring and the Aha! experience: A new model of non-monotonic problem solving, In: Vallée-Tourangeau F (ed), Insight: On the origins of new ideas, London: Routledge, 51–78.

2. Danek AH, Wiley J, Öllinger M (2016) Solving classical insight problems without Aha! experience: 9 Dot, 8 Coin, and Matchstick Arithmetic Problems. J Probl Solving 9: 47–57.

3. Bowden EM (1997) The effect of reportable and unreportable hints on anagram solution and the Aha! experience. Conscious Cogn 6: 545–573.

4. Cushen PJ, Wiley J (2012) Cues to solution, restructuring patterns, and reports of insight in creative problem solving. Conscious Cogn 21: 1166–1175.

5. Stroop JR (1935) Studies of interference in serial verbal reactions. J Exp Psychol 18: 643–662.

6. Luo J, Knoblich G (2007) Studying insight problem solving with neuroscientific methods. Methods 42: 77–86.

7. Ohlsson S (1984) Restructuring revisited: II. An information processing theory of restructuring and insight. Scand J Psychol 25: 117–129.

8. Smith SM (1995) Getting into and out of mental ruts: A theory of fixation, incubation, and insight, In: Sternberg RJ, Davidson JE (eds), The nature of insight, Cambridge, MA: MIT Press, 229–251.

9. Wertheimer M (1925) Über Schlussprozesse im produktiven Denken. In: Wertheimer M (ed), Drei Abhandlungen zur Gestalttheorie, Erlangen: Verlag der Philosophischen Akademie, 164–184.

10. Knoblich G, Ohlsson S, Haider H, et al. (1999) Constraint relaxation and chunk decomposition in insight problem solving. J Exp Psychol Learn Mem Cogn 25: 1534–1555.

11. Ohlsson S (1992) Information-processing explanations of insight and related phenomena, In: Keane MT, Gilhooly KJ (eds), Advances in the psychology of thinking, London: HarvesterWheatsheaf, 1–44.

12. Ohlsson S (2011) Deep learning: How the mind overrides experience, New York: Cambridge University Press.

13. Sandkühler S, Bhattacharya J (2008) Deconstructing insight: EEG correlates of insightful problem solving. PLoS One 3: 1–12.

14. Smith RW, Kounios J (1996) Sudden insight: All-or-none processing revealed by speed-accuracy decomposition. J Exp Psychol Learn Mem Cogn 22: 1443–1462.

15. Metcalfe J (1986) Feeling of knowing in memory and problem solving. J Exp Psychol Learn Mem Cogn 12: 288–294.

16. Metcalfe J, Wiebe D (1987) Intuition in insight and noninsight problem solving. Mem Cognit 15: 238–246.

17. Tik M, Sladky R, Luft CDB, et al. (2018) Ultra-high-field fMRI insights on insight: Neural correlates of the Aha!-moment. Hum Brain Mapp 39: 3241–3252.

18. Jung-Beeman M, Bowden EM, Haberman J, et al. (2004) Neural activity when people solve verbal problems with insight. PLoS Biol 2: 500–510.

19. Starchenko MG, Bekhtereva NP, Pakhomov SV, et al. (2003) Study of the brain organization of creative thinking. Hum Physiol 29: 652–653.

20. Bechtereva NP, Korotkov AD, Pakhomov SV, et al. (2004) PET study of brain maintenance of verbal creative activity. Int J Psychophysiol 53: 11–20.

21. Luo J, Niki K, Phillips S (2004) Neural correlates of the Aha! reaction. NeuroReport 15: 20132017.

22. Dietrich A, Kanso R (2010) A review of EEG, ERP, and neuroimaging studies of creativity and insight. Psychol Bull 136: 822–848.

23. Bowden EM, Jung-Beeman M (2003) Aha! Insight experience correlates with solution activation in the right hemisphere. Psychon Bull Rev 10: 730–737.

24. Kounios J, Beeman M (2014) The cognitive neuroscience of insight. Annu Rev Psychol 65: 7193.

25. Sprugnoli G, Rossi S, Emmendorfer A, et al. (2017) Neural correlates of Eureka moment. Intelligence 62: 99–118.

26. Luo J, Niki K, Phillips S (2004) The function of the anterior cingulate cortex (ACC) in the insightful solving of puzzles: The ACC is activated less when the structure of the puzzle is known. J Psychol Chin Soc 5: 195–213.

27. Zhao Q, Zhou Z, Xu H, et al. (2013) Dynamic neural network of insight: a functional magnetic resonance imaging study on solving chinese 'chengyu' riddles. PloS One 8: e59351.

28. Aziz-Zadeh L, Kaplan JT, Iacoboni M (2009) "Aha!": The neural correlates of verbal insight solutions. Hum Brain Mapp 30: 908–916.

29. Danek AH, Fraps T, von Müller A, et al. (2014) Working wonders? Investigating insight with magic tricks. Cognition 130: 174–185.

30. Danek AH, Öllinger M, Fraps T, et al. (2015) An fMRI investigation of expectation violation in magic tricks. Front Psychol 6: 48.

31. Danek AH, Fraps T, von Müller A, et al. (2013) Aha! experiences leave a mark: facilitated recall of insight solutions. Psychol Res 77: 659–669.

32. Ekroll V, Sayim B, Wagemans J (2013) Against better knowledge: The magical force of amodal volume completion. Iperception 4: 511–515.

33. Ekroll V, Sayim B, Wagemans J (2017) The other side of magic: the psychology of perceiving hidden things. Perspect Psychol Sci 12: 91–106.

34. Ekroll V, Sayim B, Van der Hallen R, et al. (2016) Illusory visual completion of an object's invisible backside can make your finger feel shorter. Curr Biol 26: 1029–1033.

35. Pétervári J, Danek AH (under review) Problem solving of magic tricks: Guiding to and through an impasse with solution cues.

36. Danek AH, Wiley J (2017) What about false insights? Deconstructing the Aha! experience along its multiple dimensions for correct and incorrect solutions separately. Front Psychol 7: 2077.

37. Koo TK, Li MY (2016) A guideline of selecting and reporting intraclass correlation coefficients for reliability research. J Chiropr Med 15: 155–163.

38. Nichols TE (2012) Multiple testing corrections, nonparametric methods, and random field theory. NeuroImage 62: 811–815.

39. Woo C-W, Krishnan A, Wager TD (2014) Cluster-extent based thresholding in fMRI analyses: Pitfalls and recommendations. NeuroImage 91: 412–419.

40. Eickhoff SB, Stephan KE, Mohlberg H, et al. (2005) A new SPM toolbox for combining probabilistic cytoarchitectonic maps and functional imaging data. NeuroImage 25: 1325–1335.

41. Auzias G, Coulon O, Brovelli A (2016) MarsAtlas: A cortical parcellation atlas for functional mapping. Hum Brain Mapp 37: 1573–1592.

42. Carlén M (2017) What constitutes the prefrontal cortex? Science 358: 478–482.

43. Nee DE, Brown JW, Askren MK, et al. (2013) A meta-analysis of executive components of working memory. Cereb Cortex 23: 264–282.

44. Lobel E, Kahane P, Leonards U, et al. (2001) Localization of human frontal eye fields: anatomical and functional findings of functional magnetic resonance imaging and intracerebral electrical stimulation. J Neurosurg 95: 804–815.

45. Caspers S, Eickhoff SB, Geyer S, et al. (2008) The human inferior parietal lobule in stereotaxic space. Brain Struct Funct 212: 481–495.

46. Thomas C, Didierjean A (2016) Magicians fix your mind: How unlikely solutions block obvious ones. Cognition 154: 169–173.

47. Thomas C, Didierjean A, Kuhn G (2018) It is magic! How impossible solutions prevent the discovery of obvious ones? Q J Exp Psychol 71: 2481–2487.

48. Wright RD, Lawrence MW (2008) Orienting of attention, Oxford: Oxford University Press. 49. Moore T, Fallah M (2004) Microstimulation of the frontal eye field and its effects on covert spatial attention. J Neurophysiol 91: 152–162.

50. Wang H, Callaghan E, Gooding-Williams G, et al. (2016) Rhythm makes the world go round: An MEG-TMS study on the role of right TPJ theta oscillations in embodied perspective taking. Cortex 75: 68–81.

51. Vernet M, Quentin R, Chanes L, et al. (2014) Frontal eye field, where art thou? Anatomy, function, and non-invasive manipulation of frontal regions involved in eye movements and associated cognitive operations. Front Integr Neurosci 8: 66.

52. Greicius MD, Krasnow B, Reiss AL, et al. (2003) Functional connectivity in the resting brain: A network analysis of the default mode hypothesis. Proc Natl Acad Sci 100: 253–258.

53. Kizilirmak JM, Schott BH, Thuerich H, et al. (2019) Learning of novel semantic relationships via sudden comprehension is associated with a hippocampus-independent network. Conscious Cogn 69: 113–132.

54. Gilmore AW, Nelson SM, McDermott KB (2015) A parietal memory network revealed by multiple MRI methods. Trends Cogn Sci 19: 534–543.

55. Zacks JM, Speer NK, Swallow KM, et al. (2007) Event perception: A mind-brain perspective. Psychol Bull 133: 273–293.

56. Albright TD (2012) On the perception of probable things: neural substrates of associative memory, imagery, and perception. Neuron 74: 227–245.

57. Ochsner KN, Hughes B, Robertson ER, et al. (2009) Neural systems supporting the control of affective and cognitive conflicts. J Cogn Neurosci 21: 1841–1854.

58. Botvinick MM (2007) Conflict monitoring and decision making: Reconciling two perspectives on anterior cingulate function. Cogn Affect Behav Neurosci 7: 356–366.

59. Kizilirmak JM, Thuerich H, Folta-Schoofs K, et al. (2016) Neural correlates of learning from induced insight: a case for reward-based episodic encoding. Front Psychol 7: 1693.

60. Dandan T, Haixue Z, Wenfu L, et al. (2013) Brain activity in using heuristic prototype to solve insightful problems. Behav Brain Res 253: 139–144.

61. Seghier ML (2013) The Angular Gyrus: Multiple Functions and Multiple Subdivisions. The Neuroscientist 19: 43–61.

62. Binder JR, Desai RH, Graves WW, et al. (2009) Where is the semantic system? A critical review and meta-analysis of 120 functional neuroimaging studies. Cereb Cortex 19: 2767–2796.

63. Vandenberghe R, Price C, Wise R, et al. (1996) Functional anatomy of a common semantic system for words and pictures. Nature 383: 254–6.

64. Ye Z, Zhou X (2009) Conflict control during sentence comprehension: fMRI evidence. Neuroimage 48: 280–90.

65. Spratling MW (2016) Predictive coding as a model of cognition. Cogn Process 17: 279–305.

66. Benn Y, Webb TL, Chang BPI, et al. (2014) The neural basis of monitoring goal progress. Front Hum Neurosci 8: 688.

67. Craig AD (2009) How do you feel—now? The anterior insula and human awareness. Nat Rev Neurosci 10: 59–70.

68. Tian F, Tu S, Qiu J, et al. (2011) Neural correlates of mental preparation for successful insight problem solving. Behav Brain Res 216: 626–630.

69. Boccia M, Piccardi L, Palermo L, et al. (2015) Where do bright ideas occur in our brain? Metaanalytic evidence from neuroimaging studies of domain-specific creativity. Front Psychol 6: 1195.

70. Sridharan D, Levitin DJ, Menon V (2008) A critical role for the right fronto-insular cortex in switching between central-executive and default-mode networks. Proc Natl Acad Sci 105: 12569.

71. Beaty RE, Benedek M, Barry Kaufman S, et al. (2015) Default and executive network coupling supports creative idea production. Sci Rep 5: 10964.

72. Menon V (2015) Salience Network. Brain Mapp Encycl Ref 2: 597–611.

73. Parris BA, Kuhn G, Mizon GA, et al. (2009) Imaging the impossible: An fMRI study of impossible causal relationships in magic tricks. NeuroImage 45: 1033–1039.

74. Grahn JA, Parkinson JA, Owen AM (2008) The cognitive functions of the caudate nucleus. Prog Neurobiol 86: 141–155.

75. Schneider M, Leuchs L, Czisch M, et al. (2018) Disentangling reward anticipation with simultaneous pupillometry/fMRI. Neuroimage 178: 11–22.

Instructions for Authors

Essentials for Publishing in this Journal

1 Submitted articles should not have been previously published or be currently under consideration for publication elsewhere.

2 Conference papers may only be submitted if the paper has been completely re-written (taken to mean more than 50%) and the author has cleared any necessary permission with the copyright owner if it has been previously copyrighted.

3 All our articles are refereed through a double-blind process.

4 All authors must declare they have read and agreed to the content of the submitted article and must sign a declaration correspond to the originality of the article.

Submission Process

All articles for this journal must be submitted using our online submissions system. http://enrichedpub.com/ . Please use the Submit Your Article link in the Author Service area.

Manuscript Guidelines

The instructions to authors about the article preparation for publication in the Manuscripts are submitted online, through the e-Ur (Electronic editing) system, developed by **Enriched Publications Pvt. Ltd**. The article should contain the abstract with keywords, introduction, body, conclusion, references and the summary in English language (without heading and subheading enumeration). The article length should not exceed 16 pages of A4 paper format.

Title

The title should be informative. It is in both Journal's and author's best interest to use terms suitable. For indexing and word search. If there are no such terms in the title, the author is strongly advised to add a subtitle. The title should be given in English as well. The titles precede the abstract and the summary in an appropriate language.

Letterhead Title

The letterhead title is given at a top of each page for easier identification of article copies in an Electronic form in particular. It contains the author's surname and first name initial .article title, journal title and collation (year, volume, and issue, first and last page). The journal and article titles can be given in a shortened form.

Author's Name

Full name(s) of author(s) should be used. It is advisable to give the middle initial. Names are given in their original form.

Contact Details

The postal address or the e-mail address of the author (usually of the first one if there are more Authors) is given in the footnote at the bottom of the first page.

Type of Articles

Classification of articles is a duty of the editorial staff and is of special importance. Referees and the members of the editorial staff, or section editors, can propose a category, but the editor-in-chief has the sole responsibility for their classification. Journal articles are classified as follows:

Scientific articles:

1. Original scientific paper (giving the previously unpublished results of the author's own research based on management methods).

2. Survey paper (giving an original, detailed and critical view of a research problem or an area to which the author has made a contribution visible through his self-citation);

3. Short or preliminary communication (original management paper of full format but of a smaller extent or of a preliminary character);

4. Scientific critique or forum (discussion on a particular scientific topic, based exclusively on management argumentation) and commentaries. Exceptionally, in particular areas, a scientific paper in the Journal can be in a form of a monograph or a critical edition of scientific data (historical, archival, lexicographic, bibliographic, data survey, etc.) which were unknown or hardly accessible for scientific research.

Professional articles:

1. Professional paper (contribution offering experience useful for improvement of professional practice but not necessarily based on scientific methods);
2. Informative contribution (editorial, commentary, etc.);
3. Review (of a book, software, case study, scientific event, etc.)

Language

The article should be in English. The grammar and style of the article should be of good quality. The systematized text should be without abbreviations (except standard ones). All measurements must be in SI units. The sequence of formulae is denoted in Arabic numerals in parentheses on the right-hand side.

Abstract and Summary

An abstract is a concise informative presentation of the article content for fast and accurate Evaluation of its relevance. It is both in the Editorial Office's and the author's best interest for an abstract to contain terms often used for indexing and article search. The abstract describes the purpose of the study and the methods, outlines the findings and state the conclusions. A 100- to 250-Word abstract should be placed between the title and the keywords with the body text to follow. Besides an abstract are advised to have a summary in English, at the end of the article, after the Reference list. The summary should be structured and long up to 1/10 of the article length (it is more extensive than the abstract).

Keywords

Keywords are terms or phrases showing adequately the article content for indexing and search purposes. They should be allocated heaving in mind widely accepted international sources (index, dictionary or thesaurus), such as the Web of Science keyword list for science in general. The higher their usage frequency is the better. Up to 10 keywords immediately follow the abstract and the summary, in respective languages.

Acknowledgements

The name and the number of the project or programmed within which the article was realized is given in a separate note at the bottom of the first page together with the name of the institution which financially supported the project or programmed.

Tables and Illustrations

All the captions should be in the original language as well as in English, together with the texts in illustrations if possible. Tables are typed in the same style as the text and are denoted by numerals at the top. Photographs and drawings, placed appropriately in the text, should be clear, precise and suitable for reproduction. Drawings should be created in Word or Corel.

Citation in the Text

Citation in the text must be uniform. When citing references in the text, use the reference number set in square brackets from the Reference list at the end of the article.

Footnotes

Footnotes are given at the bottom of the page with the text they refer to. They can contain less relevant details, additional explanations or used sources (e.g. scientific material, manuals). They cannot replace the cited literature.
The article should be accompanied with a cover letter with the information about the author(s): surname, middle initial, first name, and citizen personal number, rank, title, e-mail address, and affiliation address, home address including municipality, phone number in the office and at home (or a mobile phone number). The cover letter should state the type of the article and tell which illustrations are original and which are not.

Note